

AD-A 062 801
NORWAY
INTERN RAPPORT VM-61

DDESB L...

AD-A062801
INVESTIGATION OF UNDERGROUND EXPLOSIONS
WITH MODEL TESTS
MEASUREMENTS ON THE PLATFORM

by

S Rollvik and M Vigstad

AUG 1978

This document has been approved
for public release and sale; its
distribution is unlimited.

FORSVARETS FORSKNING SINSTITUTT
NORWEGIAN DEFENCE RESEARCH ESTABLISHMENT
P O Box 25 - N-2007 Kjeller, Norway

79 05 11 081

~~78 12 21 024~~

DISCLAIMER NOTICE

**THIS DOCUMENT IS BEST QUALITY
PRACTICABLE. THE COPY FURNISHED
TO DDC CONTAINED A SIGNIFICANT
NUMBER OF PAGES WHICH DO NOT
REPRODUCE LEGIBLY.**

FFIVM

Intern rapport VM-61

Reference: 261/130:738

Date: August 1978

AD-A062801

INVESTIGATION OF UNDERGROUND EXPLOSIONS WITH MODEL TESTS

MEASUREMENTS ON THE PLATFORM

by

S Rollvik and M Vigstad

Approved
Kjeller 31 August 1978

T. Krog
T Krog
Superintendent



FORSVARETS FORSKNINGSINSTITUTT

Norwegian Defence Research Establishment

P O Box 25 - N-2007 Kjeller

Norway

79 05 11 081

CONTENTS

	Page
1 INTRODUCTION	4
2 DIFFICULTIES WITH PRESSURE TRANSDUCERS	5
3 TUBE OUTLET	6
3.1 Scale-dependence of the pressure drop	6
3.2 Examination of the pressure drop	6
3.3 Conclusion	7
4 CURVE FITTING ON PRESSURES OBTAINED FROM TIME MEASUREMENTS	8
4.1 Curve fitting procedure	8
4.2 Discussion of P_o	8
4.3 Discussion of B	9
4.3.1 Dependence of B on scale	10
4.3.2 Dependence of B on roughness	10
4.4 Results from front-pressure measurements	10
5 FITTING OF EMPIRICAL EQUATIONS TO ARRIVAL TIME DATA	11
5.1 Comparison between curve forms	11
5.2 Fitting of eq (5.2) to the measured arrival times	13
5.3 Discussion of A_o/B_o	13
5.3.1 Dependence of A_o/B_o on q	13
5.3.2 Dependence of A_o/B_o on r_L	14
5.3.3 Dependence of A_o/B_o on D^L	14
5.4 Discussion of DR_o	15
5.4.1 Dependence of DR_o on q	15
5.4.2 Dependence of DR_o on r_L	15
5.4.3 Dependence of DR_o on D^L	16
5.5 Fitting of eq (5.1) to the measured arrival times	16
5.6 Discussion of U_o	17
5.6.1 Dependence of U_o on q	17
5.6.2 Dependence of U_o on r_L	17
5.6.3 Dependence of U_o on D^L	17
5.7 Discussion of DR_o	18
5.7.1 Dependence of DR_o on q	18
5.7.2 Dependence of DR_o on r_L	18
5.7.3 Dependence of DR_o on D^L	18
5.8 Summary	18

		Page
6	THE 50 mbar LIMIT	19
6.1	Determination of the 50 mbar limit	19
6.2	Discussion of x	19
6.2.1	Dependence of x on q	19
6.2.2	Dependence of x on r_L	20
6.2.3	Dependence of x on D^L	20
7	COMPARISON WITH FULL-SCALE TESTS	21
8	CONCLUSIONS	23
	References	24
	Figures	25-32
	Tables	33-65

INVESTIGATION OF UNDERGROUND EXPLOSIONS WITH MODEL TESTS

Measurements on the platform

SUMMARY

Model tests in three scales were undertaken to examine if simple scaling laws can be used to investigate underground explosions. Charges were detonated in steel tubes, and pressures and arrival times were measured in the tube and on a platform. The objective of the tests is described in more detail in (1), which also describes the results from the measurements in the tube.

This report describes the results from the measurements on the platform. As for the measurements in the tube, a deviation from the simple scaling laws is observed. The dependence of the pressure on tube diameter, charge weight and wall roughness is examined.

A detailed description of the experimental set-up is given in (2) and of the data processing in (3). Reference (3) also contains a list of the measured front pressures, maximum pressures and arrival times.

1. INTRODUCTION

Model tests in three scales were undertaken to examine if simple scaling laws are valid for describing the blast wave originating from an accidental explosion in an underground ammunition storage site. The objective of the tests is described in more detail in (1). The models consist of a tube, simulating a tunnel, and a platform, simulating flat terrain (1,2). The pressure-time history of the blast and the arrival time of its shock front were measured and recorded (2,3). The results from the measurements in the tube section were presented and discussed in (1). In this report the results from the measurements on the platform section are discussed. The necessary definitions for reading this report are also found in (1).

In the appendix to (3), all the recorded front pressures, maximum pressures and arrival times, both from the tube section and from the platform section, are listed.

2 DIFFICULTIES WITH PRESSURE TRANSDUCERS

The pressures measured on the platform range from a few bar close to the tube outlet to about 50 mbar at larger distances from the outlet. It is difficult to find good pressure transducers which cover this range of values.

We have used LC65 transducers from Celesco. The uncertainties in the measurements with these should be about 20%. In addition to this uncertainty, there are oscillations in the platform which may disturb the measurements.

When the experiments were finished, it was realized that the calibration values of the transducers as given by the producer were unsatisfactory. Control calibrations performed at the Norwegian Defence Research Establishment showed a deviation of about 100% from those given by the producer. No information about linearity is given by the producer.

As a result of this uncertainty with the calibration, the discussion in this report is based mainly on the arrival time measurements.

However, for some of the pressure transducers, it was possible to establish a confident calibration procedure. As a result it was possible to recalculate the front pressure at the measurement stations closest to the tube outlet in CFG.1, and for the case of zero wall roughness in CFG.1 even at most of the measurement stations. The front pressures obtained in this way are used with some confidence.

In the listing of the pressures in the appendix of (3) the uncorrected pressure values are given.

3 TUBE OUTLET

3.1 Scale-dependence of the pressure drop

In (1) we observed that the front pressures in the tube were larger in the larger scales, and that the difference increased with distance from the charge. When we look at the front pressures at the measurement station 10 tube diameters from the tube outlet on the platform (Table 3.1), it is therefore surprising to find that the front pressures now are smaller in the larger scales. The deviation from scaling with respect to dimension seems to change direction when passing through the tube outlet. Figure 3.1 shows some examples of how the front pressure falls as it passes through the outlet in the three scales. We shall study in greater detail the pressure drop of the shock front when it passes through the tube outlet. This pressure drop is due to the fact that the propagation of the shock wave changes from one-dimensional to three-dimensional.

Since on the platform we have confidence only in the pressure measurements in CFG.1, we shall restrict ourselves to this configuration.

3.2 Examination of the pressure drop

We have calculated

$$\gamma = \frac{P'}{P''} \quad (3.1)$$

where P' is the front pressure at position $n=52$ in the tube just at the outlet, and P'' is the pressure at the position $N=10$ tube diameters from the outlet on the platform. P' increases with increasing scale, while P'' decreases with increasing scale.

The values of γ are listed in Table 3.2.

To study the deviation of γ with increasing D , the values of γ are used to estimate a linear equation

$$\gamma = a + bD \quad (3.2)$$

The values of a and b and the correlation coefficient R are listed in Table 3.3. b is positive, indicating that the pressure drop increases when D increases. It is also seen as a weak tendency that b decreases when the charge group q increases. The scale dependence of the pressure drop is thus larger for smaller charges than for larger charges.

From Table 3.2 we also see that γ decreases when q increases, and that it increases with increasing large-scale roughness.

3.3 Conclusion

The large-scale roughness of the tube walls influences the pressure drop in a region where it is not physically present. The wall roughness must thus influence the pressure drop through its earlier impact on the pressure-time history of the blast following the front shock, as it propagates through the tube. It must be concluded from this, and from the discussion in section 3.2, that the drop in front pressure through the tube outlet depends critically on the pressure-time history following the shock, and that the scale dependence of the pressure drop must result from a scale dependence of this pressure-time history. This shows that if one wants to get a clear picture of the front pressure dependence on scale, one must examine how other parameters describing the blast, such as impulse and positive duration, depend on scale.

We have not analysed our pressure/time plots sufficiently to give any conclusions about the scale dependence of impulse or positive duration, and shall not comment on which physical effects are determining the pressure drop. As will be seen from the discussion of the shock propagation on the platform, however, the scale dependence of the pressure drop in the tube outlet does not seem to result from a scale dependent loss of energy in this region, but from a scale dependent redistribution of energy in the blast.

4 CURVE FITTING ON PRESSURES OBTAINED FROM TIME MEASUREMENTS

4.1 Curve fitting procedure

Based on measurements of arrival times a mean velocity of the shock between two succeeding measurement stations are calculated. We let this velocity correspond to a position midway between the two measurement stations. The front-pressure in this position is then calculated by the Rankine-Hugoniot equation. The curve from

$$P = P_0 \left(\frac{N}{20} \right)^{-B} \quad (4.1)$$

where N is the distance from the tube outlet, measured in number of tube diameters, is fitted to the values of the front pressures. The fitting parameters P_0 and B represent the pressure in position $N = 20$ and the attenuation of the front pressure, respectively. Only pressures in positions $N > 20$ are included in the curve fitting.

The values of P_0 , B and the correlation coefficient R are shown in Table 4.1a for CFG.1 and Table 4.1b for CFG.2.

4.2 Discussion of P_0

It is seen that P_0 increases with increasing q , but that the increase is smaller than a linear increase. The curve form

$$P_0 = a e^{bq} \quad (4.2)$$

is with good correlation fitted to the values of P_0 . The results are shown in Table 4.2a for CFG.1 and Table 4.2b for CFG.2.

For each configuration and each degree of the large scale wall roughness r_L , b seems to be independent of D . It decreases, however, with increasing r_L . That is, while the increase in P_0 with increasing charge group seems to be independent of scale, it is smaller for larger values of wall roughness.

From Table 4.2 it is seen that a , on the average, decreases with increasing r_L . It is also seen that a decreases with increasing D , and this de-

crease seems to be larger for larger values of r_L . It follows that P_o decreases with increasing r_L and D , and that the decrease in P_o is larger for larger values of r_L . This is consistent with the observations in chapter 3.

4.3 Discussion of B

From Table 4.1 it is seen that B is nearly independent of q , indicating that the attenuation of the front pressure on the platform is nearly independent of q .

The equation

$$B = b_1 + b_2 D + b_3 r_L \quad (4.4)$$

is by linear regression fitted to the values of B . The resulting values of b_1 , b_2 and b_3 and the corresponding partial correlation coefficients are given in Table 4.3a for CFG.1 and Table 4.3b for CFG.2. All the correlation coefficients are significant on a level $\epsilon = 10\%$.

With the values of the b -parameters inserted in Equation (4.4), we obtain

$$B = 1.75 - 2.70 D - 5.39 r_L \quad (4.5a)$$

for CFG.1, and

$$B = 1.52 - 2.01 D - 4.20 r_L \quad (4.5b)$$

for CFG.2.

We tried to include a term $b_4 r_L D$ in Equation (4.4) to examine the interaction between roughness and scale. The resulting values of b_4 were negative both for CFG.1 and CFG.2, but the correlation coefficients were not significant.

4.3.1 Dependence of B on scale

The first thing we notice is that B decreases when D increases; that is, the attenuation of the front pressure is smaller in the larger scales. We have observed that P_0 , the front pressure in position N = 20, decreases with increasing scale. The situation can then be summarized as follows:

In the tube, the front pressure is larger in the larger scales. When the shock wave propagation changes from one-dimensional to three-dimensional in the tube outlet, there is a large pressure drop, and this pressure drop is so much larger in the larger scales that in position N = 20 on the platform, the front pressure is largest in the smallest scales. As the shock propagates on the platform, however, the front pressure decreases more in the smaller scales, until it eventually becomes smallest in the smaller scales. This shows that the scale dependence of the pressure drop as the shock front passes through the tube outlet, is not due to a scale dependent energy loss, but a scale dependent redistribution of energy.

4.3.2 Dependence of B on roughness

We see that B decreases when r_L increases. The effect of the wall roughness in the tube on the attenuation of the front pressure on the platform must be through its effect on the shape of the pressure-time profile of the blast as this propagates through the tube. A small attenuation corresponds to a flat pressure-time profile. The effect of the roughness in the tube must be to flatten the pressure time profile which again results in a smaller attenuation of the front pressure on the platform.

4.4 Results from front pressure measurements

As mentioned in chapter 2 the uncertainty in the calibration of the pressure gauges is generally too great for the pressure measurements to be used with confidence. For $r_L = 0$ in CFG.1, however, the necessary corrections have been made, and the resulting values of the front pressures are listed in Tables 4.4a-c.

Equation (4.1) is fitted to these front pressure values, and the resulting values of P_0 and B, and the correlation coefficients, R, are also listed in the Tables 4.4.

Equation (4.2) is fitted to the obtained values for P_o , and the results are

$$P_o = 0.187 e^{0.0030 q} \quad \text{with correlation } R = 1.00$$

for scale 1:100,

$$P_o = 0.255 e^{0.0022 q} \quad \text{with } R = 0.99$$

for scale 2:100, and

$$P_o = 0.217 e^{0.0025 q} \quad \text{with } R = 0.98$$

for scale 3:100.

When this is compared with the corresponding results from the front pressures obtained from arrival time measurements, section 4.2, Table 4.2, it is seen to be a fair agreement as far as attenuation is concerned. However, the absolute values are appreciably lower.

As is the case for curve fitting based on front pressures obtained from time measurements, B in Equation (4.1) is seen to be nearly independent of q also in the curve fitting based on the measured front pressures. The mean value of B in each scale in the latter case corresponds reasonably well with the values in the former case.

5 FITTING OF EMPIRICAL EQUATIONS TO ARRIVAL TIME DATA

In chapter 4 the measured arrival times were used to calculate the front pressures, and a curve fitting procedure was performed on the front pressures. In this chapter the curve fitting will be performed on the measured arrival times directly.

5.1 Comparison between curve forms

Three expressions have been fitted to the arrival times measured in positions with $N > 20$ on the platform. The expressions are the following

$$(t-t_0) = \beta_1(N-20) + \beta_2(N-20)^2 + \beta_3(N-20)^3 \quad (5.1)$$

$$D(N-20) = a_0(t-t_0) + A_0 \ln \left(1 + \frac{t-t_0}{B_0}\right) + D_0 \quad (5.2)$$

$$D(N-20) = a_0(t-t_0) + A_0 \left\{ \ln \left(1 + \frac{t-t_0}{B_0}\right) \right\}^{\frac{1}{2}} \quad (5.3)$$

t_0 is the arrival time at position $N = 20$. a_0 is the speed of sound in the undisturbed air ahead of the shock front. β_1 , β_2 , β_3 , A_0 , B_0 and D_0 are fitting parameters.

There is no physical reason for equation (5.1); it is only a fitting equation. Equations (5.2) and (5.3) have at least the property that the shock velocity approaches the velocity of sound, as time approaches infinity. Expressions similar to equations (5.2) and (5.3) were, among others, discussed for spherical explosions in free air in a paper by T K Groves at Suffield Experimental Station (4).

To decide which of these three expressions that give the best fit to the measured arrival times, a method described by Dylewski in (5) is used.

For each shot the curve forms are fitted to the observed arrival times, and the square deviation S is calculated for all the three curves. Then the measured arrival times in the measurement stations nearest to the tube outlet are fitted to the data and the square deviation S' is calculated for the three curve forms. In the same way the square deviation S'' for the fitting of the remaining arrival time measurements is calculated for the three expressions. The curve form giving the smallest value of $S/S'+S''$ is the best one by this criterion.

This has been done for each shot. For equation (5.2) this has been performed also with the parameter D_0 excluded. (In this case the expression has the property that $L = L_0$ when $t = t_0$). The results when D_0 was excluded and when D_0 was included turned out to be equally good. Each gave the smallest value of $S/S'+S''$ in about 50% of the shots.

In 80% of the shots equation (5.2) is a better fit than equation (5.1), and in 90% of the shots equation (5.2) is better than equation (5.3). Thus, equation (5.2) turns out to fit best to the observed arrival times.

We shall in the following sections present the results of the fitting of equation (5.2) to the data when the parameter D_0 is included. In sections 5.5 to 5.7 the results from the fitting of equation (5.1) to the data will be presented.

5.2 Fitting of equation (5.2) to the measured arrival times

A_0 , B_0 and D_0 have been calculated for each shot, and listed in Tables 5.1a and b. The values of S and $S/(S'+S'')$ are also listed in this table.

From equation (5.2) the shock velocity is given by the equation

$$U = \frac{dL}{dt} = a_0 + \frac{A_0}{B_0 + (t - t_0)} \quad (5.4)$$

and the acceleration is

$$\frac{dU}{dt} = - \frac{A_0}{(B_0 + (t - t_0))^2} \quad (5.5)$$

In position $L = 20$, where $t = t_0$, the shock velocity exceeds the velocity of sound with an amount A_0/B_0 , and its retardation is $R_0 = A_0/B_0^2$. When we shall study the dependence of the shock on scale, charge group and roughness, we shall take A_0/B_0 as a measure of the shock strength in position $N = 20$, and DR_0 to represent the attenuation of the shock.

The values of A_0/B_0 and DR_0 are calculated for each shot. We shall in the following sections take the values of A_0/B_0 and DR_0 from each shot and fit simple curve forms to them, in order to study their qualitative behaviour.

5.3 Discussion of A_0/B_0

5.3.1 Dependence of A_0/B_0 on q

The equation

$$\frac{A_0}{B_0} = a e^{bq} \quad (5.6)$$

is fitted to the values of A_o/B_o , and the resulting values of a , b and the correlation coefficient R are listed in Table 5.2a for CFG.1 and Table 5.2b for CFG.2. b is positive, showing that the shock strength in position $N = 20$ increases with increasing charge weight. b is seen to decrease with increasing roughness. This is consistent with what was observed in section 4.2.

Figure 5.1 shows an example on the dependence of A_o/B_o on q .

5.3.2 Dependence of A_o/B_o on r_L

The equation

$$\frac{A_o}{B_o} = a + br_L \quad (5.7)$$

is fitted to the values of A_o/B_o , and the results are given in Table 5.3a for CFG.1 and in Table 5.3b for CFG.2. b is seen to be negative; that is, the shock strength at $N = 20$ decreases with increasing roughness. This decrease is larger for the larger charge groups.

These results are similar to those obtained in section 4.2. Some examples on the dependence of A_o/B_o on r_L are shown in Figure 5.2.

5.3.3 Dependence of A_o/B_o on D

The equation

$$\frac{A_o}{B_o} = a + bD \quad (5.8)$$

is fitted to the values of A_o/B_o . The results are given in Table 5.4a for CFG.1 and Table 5.4b in CFG.2. As in section 4.2, a tendency of the shock strength at $N = 20$ to decrease with increasing scale is observed. ($b < 0$ in 29 of 33 cases). This tendency seems to be stronger for the larger charge groups. It is difficult, however, in this case to see any dependence of b on r_L .

Figure 5.3 shows some examples on the dependence A_o/B_o on D .

5.4 Discussion of DR_0

$DR_0 = D A_0 / B_0^2$ is taken to represent the decay in the shock strength as the blast propagates over the platform. The dependence of DR_0 on charge group, wall roughness in the tube and scale will now be discussed.

5.4.1 Dependence of DR_0 on q

The equation

$$DR_0 = a e^{bq} \quad (5.9)$$

is fitted to the values of DR_0 . The results are listed in Table 5.5a for CFG.1 and Table 5.5b for CFG.2.

In section 4.3 the attenuation of the front pressure was found to be nearly independent of q . From Table 5.5 it is seen, on the contrary, that $b > 0$ in 14 of 18 cases, indicating that the decay in the shock strength increases with increasing charge group. However, no systematic dependence of this increase on wall roughness and scale is observed.

Figure 5.4 shows an example on the dependence of DR_0 on q .

5.4.2 Dependence of DR_0 on r_L

The results from fitting the equation

$$DR_0 = a + br_L \quad (5.10)$$

to the values of DR_0 are given in Table 5.6a for CFG.1 and Table 5.6b for CFG.2. In 30 of 32 cases b is found to be negative indicating that the decay in shock strength is smaller for the larger values of wall roughness. This effect was also observed in section 4.3.

b is seen to decrease with increasing charge group. It then follows that the effect of smaller attenuation of the shock with increasing roughness, is larger for larger charge groups.

Figure 5.5 shows some examples on the dependence of DR_0 on r_L .

5.4.3 Dependence of DR_0 on D

The equation

$$DR_0 = a + bD \quad (5.11)$$

is fitted to the values of DR_0 . The results are given in Table 5.7a for CFG.1 and Table 5.7b for CFG.2. In 30 of 33 cases b is negative. This shows that the decay of the shock strength decreases with increasing scale. The similar result was obtained in section 4.3.

b seems to decrease with increasing charge group. It means the decrease of the attenuation with increasing scale is larger for larger charge groups. The tendency here, however, is weak.

Some examples of the dependence of DR_0 on D are shown in Figure 5.6.

5.5 Fitting of equation (5.1) to the measured arrival times

We shall also briefly present the results from the fitting of equation (5.1) to the measured arrival times. t_0 in equation (5.1) is taken to be the measured arrival time in position $N = 20$. From equation (5.1) the velocity of the shock front is given by

$$U = D \frac{dN}{dt} = D(\beta_1 + 2\beta_2(N-20) + 3\beta_3(N-20)^2)^{-1} \quad (5.12)$$

and its acceleration is

$$\frac{dU}{dt} = -D(\beta_1 + 2\beta_2(N-20) + 3\beta_3(N-20)^2)^{-3}(2\beta_2 + 6\beta_3(N-20)) \quad (5.13)$$

The shock velocity at $N = 20$ is then

$$U_0 = \frac{D}{\beta_1} \quad (5.14)$$

and the retardation is

$$R_0 = + \frac{2D\beta_2}{\beta_1^3} \quad (5.15)$$

Since our main interest now is to compare the results from the fitting of equation (5.1) to the measured arrival times with the results from the fitting of equation (5.2), we shall concentrate the discussion on U_0 and the "scaled" retardation in $N = 20$, DR_0 . It must be borne in mind, however, that there is an additional parameter β_3 .

The values of U_0 , DR_0 and β_3 are given in Table 5.8a for CFG.1 and Table 5.8b for CFG.2.

5.6 Discussion of U_0

5.6.1 Dependence of U_0 on q

The equation

$$U_0 = a e^{bq} \quad (5.16)$$

is fitted to the values of U_0 , and the results are listed in Table 5.9a for CFG.1 and Table 5.9b for CFG.2. As in section 5.3.1 b is found to be positive, and it has a tendency to decrease with increasing wall roughness and scale.

5.6.2 Dependence of U_0 on r_L

The equation

$$U_0 = a + br_L \quad (5.17)$$

is fitted to the values of U_0 and the results are given in Tables 5.10. b is found to be negative, and it has larger negative values for larger charge groups.

The results are similar to those observed in section 5.3.2.

5.6.3 Dependence of U_0 on D

The results from fitting the equation

$$U_0 = a + bD \quad (5.18)$$

to the values of U_0 are listed in Tables 5.11. b is negative in 23 of 33 cases, so the tendency of the shock strength in $N = 20$ to decrease with increasing scale is observed also in this case. As in section 5.3.3 this tendency seems to be stronger for larger charge groups.

5.7 Discussion of DR_0

5.7.1 Dependence of DR_0 on q

Equation (5.9) is fitted to the values of DR_0 and the results are listed in Tables 5.12. As in section 5.4.1 a weak tendency of DR_0 to increase with increasing charge group is observed. It is difficult to see any systematic dependence of this increase on scale and roughness.

5.7.2 Dependence of DR_0 on r_L

Equation (5.10) is fitted to the values of DR_0 , and the results are listed in Tables 5.13. DR_0 is found to decrease with increasing r_L , just as in section 5.4.2. A weak tendency of this decrease to become larger for larger charge weights is also observed, while it is difficult to find any dependence on D .

5.7.3 Dependence of DR_0 on D

At last, equation (5.11) is fitted to the values of DR_0 , and from the results, listed in Tables 5.14, DR_0 does not, as in section 5.4.3, show any tendency to decrease with increasing scale. This difference is due to the additional fitting parameter β_3 in Equation (5.1). When the scale-dependence of this parameter is taken into account, the retardation of the shock front, and hence the attenuation of the front pressure, is found to decrease with increasing scale.

5.8 Summary

In this and the preceeding chapter several curve fitting procedures were performed to interpret the arrival time measurements. They give all the same qualitative results. This assures that the conclusions are not only

resulting from the curve fitting procedures used, but reveal the physical content of the data.

The main results can be summarized as follows: At the beginning of the platform ($N = 20$), the front pressure increases with increasing charge group, and decreases with increasing scale and roughness. The attenuation of the front pressure, however, also decreases with increasing scale and roughness.

6 THE 50 mbar LIMIT

6.1 Determination of the 50 mbar limit

It is of interest to find the distance from the tube outlet in which the front pressure falls below a certain value, for example 50 mbar. Since equation (5.2) gives the best fit to the measured arrival times, this will be used to determine the 50 mbar limit.

By use of equation (5.2) and the Rankine-Hugenoit equation, the 50 mbar limit is found to be expressed as

$$x = 20 + \frac{1}{D} \{ 47.8 A_o - a_o B_o + A_o \ln(47.8 \frac{A_o}{a_o B_o}) + D_o \} \quad (6.1)$$

x measures the distance in number of tube diameters. The values of x obtained by Equation (6.1) are listed in Table 6.1 for the different charge groups, degrees of wall roughness and scales.

6.2 Discussion of x

6.2.1 Dependence of x on q

The equation

$$x = a q^b \quad (6.2)$$

is fitted to the values of x , and the results are given in Table 6.2a for CFG.1 and Table 6.2b for CFG.2. All the values of b are found to be be-

tween 0 and 1, i e, about 0.4 for CFG.1 and 0.5 for CFG.2, showing that x increases with increasing q . Figure 6.1 shows an example on the dependence of x on q .

It is difficult to find any dependence of b on D and r_L .

6.2.2 Dependence of x on r_L

The equation

$$x = a + br_L \quad (6.3)$$

is fitted to the values of x , and the results are given in Table 6.3. b is found to be negative in 26 of 33 cases, indicating that x decreases with increasing roughness in the tube. The decrease seems to be larger for the larger charge groups.

As discussed in the preceeding chapters, the effect of the wall roughness in the tube is to flatten the pressure-time profile of the blast. This leads to smaller values of the front pressure at the beginning of the platform in the cases of large roughness, but also to smaller attenuation of the front pressure as the shock propagates over the platform. For the 50 mbar limit the effect of the roughness still is to give smaller values of x with larger degrees of roughness.

In Figure 6.2 are shown some examples on the dependence of x on r_L .

6.2.3 Dependence of x on D

The equation

$$x = a + bD \quad (6.4)$$

is fitted to the values of x . The results are listed in Tables 6.4.

b is positive in 26 of 33 cases, showing that the distance to the point where the pressure falls below 50 mbar increases with increasing scale. $b > 0$ in 24 of 33 cases is a relative weak tendency. This is probably due to the effect of the tube outlet. The front pressure in position $N = 20$ on the platform was found to decrease with increasing scale. The attenuation of the front pressure as the shock propagates over the plat-

form, was, however, also found to decrease with increasing scale, so that for larger values of N increasing front pressure with increasing scale is observed. The value of N for which this occurs, will depend on the pressure-time profile of the blast, but no systematic analysis of this has been performed.

Figure 6.3 shows some examples on the dependence of x on D .

7

COMPARISON WITH FULL SCALE TESTS

We shall briefly compare the results obtained in Norwegian full scale tests at Raufoss and Storfosen with the present model tests. The Raufoss and Storfosen experiments are described in (6) and (7), respectively. There are large differences both in charge groups used and in geometry between these full scale tests and the model experiments. This makes a direct comparison difficult. Except for one shot, where a direct comparison is performed, we have therefore only taken the front pressures obtained in the Raufoss- and Storfosen shots and fitted equation (4.1) to them. The results are given in Table 7.1. The curve fitting is based on measurements in 2, 4 or 5 positions outside the tunnel outlet, N being between 10 and 80.

The tunnel diameter at Raufoss is $D = 2.65$ m, corresponding to scale 53:100. At Storfosen 2 tunnels were used. Both tunnels had bends, and in both tunnels the diameter changed. We shall associate a diameter $D = 2.85$ m to the one and a diameter $D = 4$ m to the other, corresponding to scales 57:100 and 80:100, respectively.

In the discussion in section 4.3 the attenuation B was found to decrease with increasing scale. By comparing the values of B from the full scale case in Table 7.1 with the values of B from the model tests in Tables 4.1, the attenuation in the full scale tests is of the same order of magnitude or somewhat smaller. This may be due to the different values of charge group q , although in section 4.3. B was found to be nearly independent of q .

By comparing the values of P_0 from Table 7.1 with the values of P_0 from

Table 4.1, P_0 is found to be smaller in the full scale tests. This is reasonable, since the charge groups are smaller in the full scale tests.

As mentioned there are several important differences between these full scale experiments and the model tests, and this makes a direct comparison difficult. It is shot no 9 from Raufoss which is best suited for a direct comparison, and even in this case the differences are large. The charge weight in this shot is $Q = 1000$ kg, corresponding to charge group $q = 53.7$ kg/m³. The pressure as a function of distance from the tunnel outlet is shown in Figure 7.1. The Raufoss tunnel is closed in one end, as our CFG.2, and the charge is detonated in the tunnel, as in our CFG.1. The Raufoss shot should then be compared with shots with charge group 2×53.7 kg/m³ ≈ 107 kg/m³ in CFG.1 in our model tests. We have not used exactly this charge group, but a comparison can be performed by interpolation from the shots with $q = 80$ kg/m³ and $q = 160$ kg/m³. The resulting pressures as function of distance from tube outlet for scales 1:100, 2:100 and 3:100 are also shown in Figure 7.1. It is assumed that $r_L = 0.06$ is the wall roughness which best corresponds to the roughness in the Raufoss tunnel.

As is seen in Figure 7.1, that while the pressure increases with increasing scale in the model tests, the pressure is much lower in the Raufoss shot.

It seems reasonable to explain this deviation between the model tests and the Raufoss shot by the larger differences between the full scale case and the models, of which the most important are:

- A possibly larger large-scale and small-scale roughness in the rock tunnel at Raufoss
- Vegetation and irregularities in the terrain might be of greater importance than irregularities on the platform
- There is a side-chamber and a bend in the Raufoss tunnel
- Energy in the blast wave is used for evaporation of water in the tunnel
- In the models there are a vertical steel plate above the tube outlet, while at Raufoss the hill above the tunnel is not very steep
- The tunnel length at Raufoss is only 34 tunnel diameters; the effect of this, however, should be in the opposite direction

CONCLUSIONS

For the measurements in the tube section a deviation from the scaling laws was observed (1). It was seen that the front pressure increased with increasing scale, mainly due to the fact that the attenuation of the front pressure decreased with increasing scale.

In chapter 3 of the present report the tube outlet was seen to have the effect of reversing this deviation; at the first measurement stations after the tube outlet the front pressure decreased with increasing scale. In other words, there is a larger pressure drop in the larger scales, when the shock propagation changes from one-dimensional in the tube to three-dimensional on the platform. This effect was seen to depend on the wall roughness in the tube, indicating that the pressure-time profile of the blast is of importance for the magnitude of the effect.

The effect does not seem to result from a scale dependent loss of energy in the tube outlet, but rather from a scale dependent redistribution of energy. The attenuation of the front pressure as the shock propagates over the platform is smaller in the larger scales, and at sufficiently large distances from the tube outlet the front pressure increases with increasing scale. This effect makes it difficult to extrapolate the scale dependence of the 50 mbar-limit, for example, to large scales.

In chapters 4 and 5 where the dependence of the attenuation of the front pressure and the front pressure in position $N = 20$ on scale, charge group and roughness was studied, the attenuation was found to depend on the roughness in the tube. This again shows the importance of the whole pressure-time history for describing the blast.

The time frame of this project has not made a study of the pressure-time profiles possible, although they are recorded.

In summary, a relative complicated dependence of the shock strength on scale is observed. This supports the conclusion in (1), that the simple scaling laws must be used with great care.

References

- (1) Rollvik, S
M Vigstad
 - Investigation of underground explosions with model tests: Measurements in the tube, Intern rapport VM-60, Norwegian Defence Research Establishment (1978)
- (2) Skarbøvik, K
M Vigstad
 - Investigation of underground explosions with model tests: The experimental set-up, Teknisk notat VM-309, Norwegian Defence Research Establishment (1978)
- (3) Christoffersen, Ø
 - Investigation of underground explosions with model tests: System description and some implementation details, Teknisk notat S-498, Norwegian Defence Research Establishment (1978)
- (4) Groves, T K
 - The measurements of air blast pressure in TNT explosions with special reference to an explosion of 100 tons TNT at ground level (U), Suffield Technical Paper no 255 (1964)
- (5) Dylewski, T J
 - Criteria for selecting curves for fitting to data, AIAA Journal 8, 8 (1970)
- (6) Strømspøe, E
 - Underground explosion trials at Raufoss 1968 - Measurements of air blast outside the tunnel, Intern rapport X-124, Norwegian Defence Research Establishment (1969)
- (7) Curran, D R
 - Air-shock overpressures outside tunnels in which detonations have occurred, Intern rapport X-117, Norwegian Defence Research Establishment (1967)

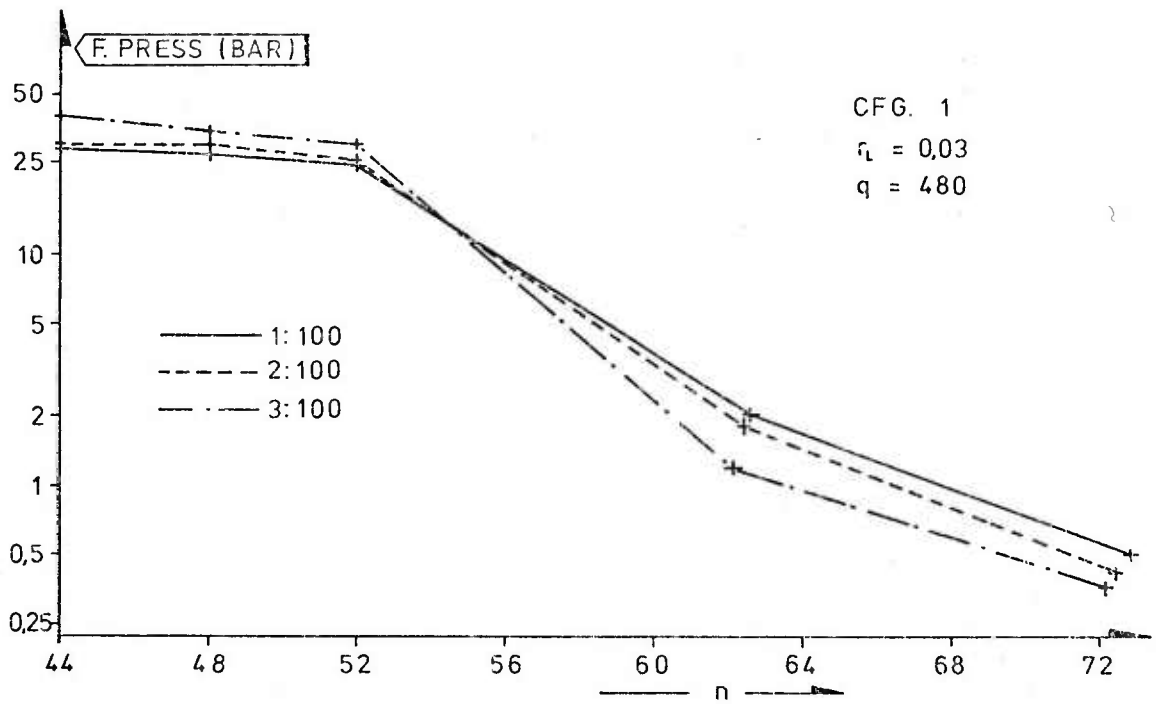


Figure 3.1a Pressure drop in the tube outlet

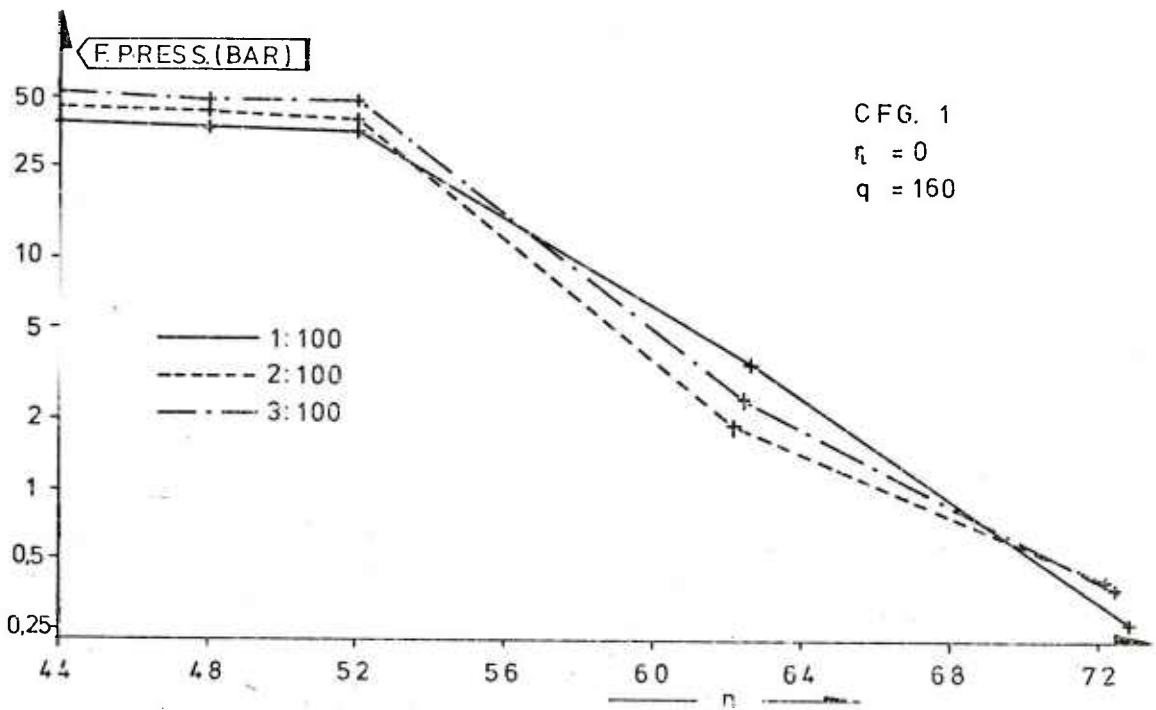


Figure 3.1b Pressure drop in the tube outlet

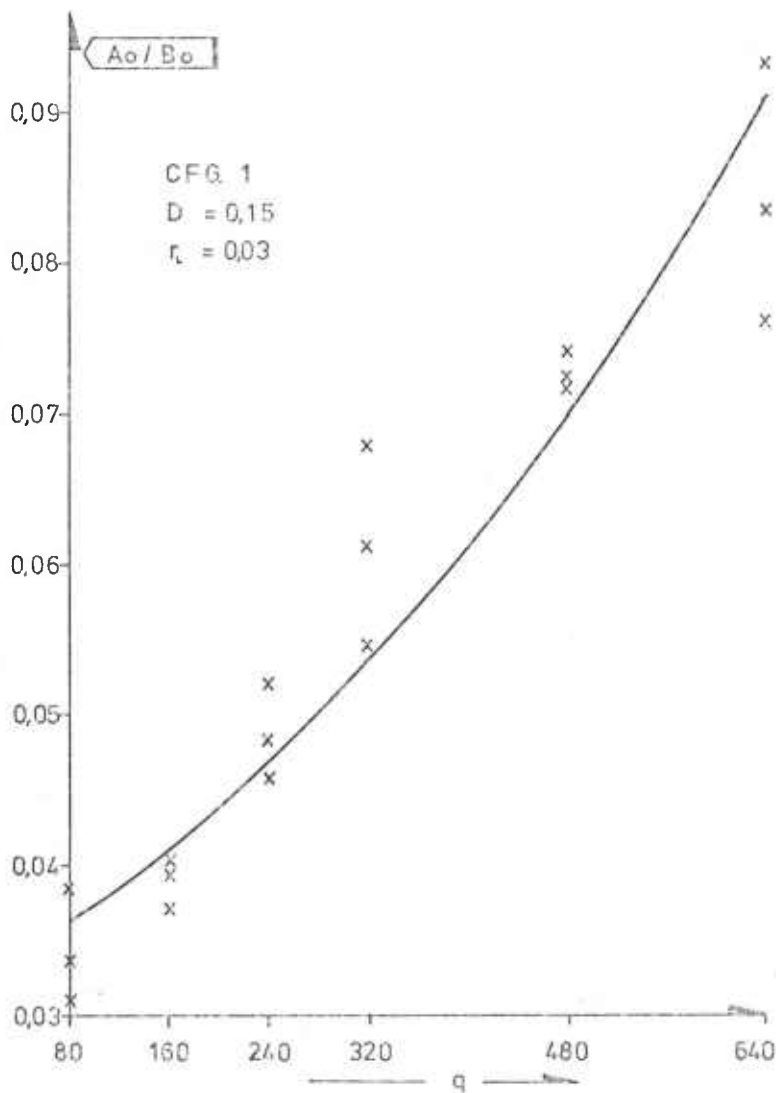


Figure 5.1 A_o/B_o as function of charge group, q
 (The curve is the result from fitting eq (5.6) to the values of A_o/B_o)

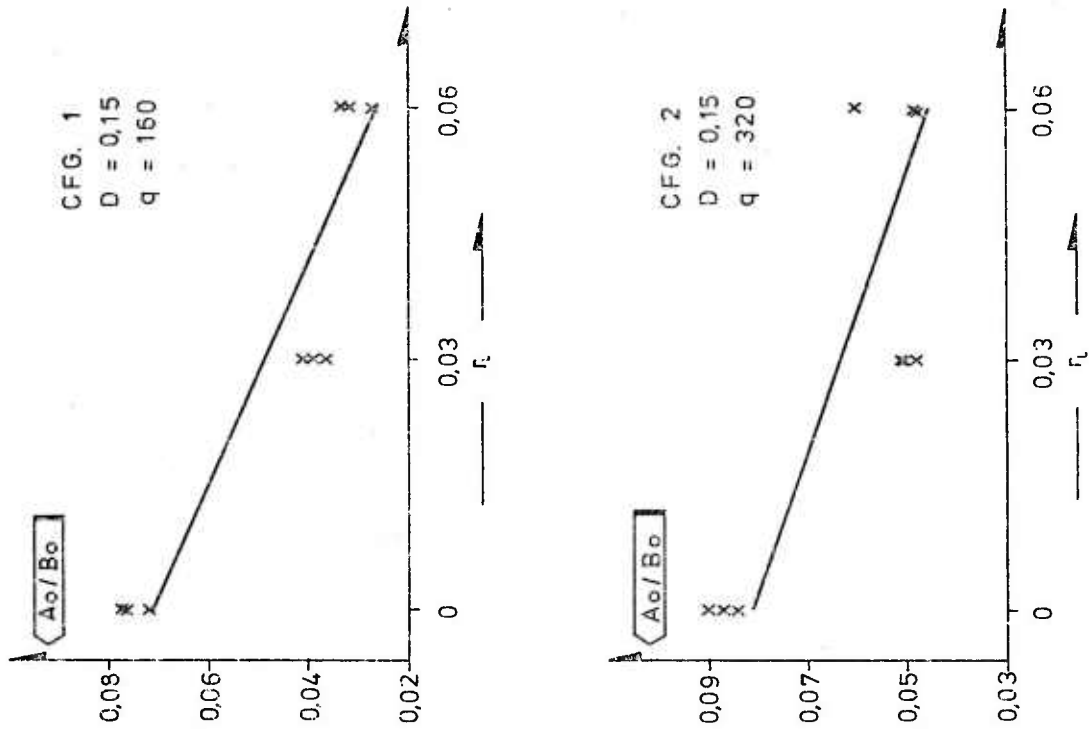


Figure 5.2 A_o/B_o as function of wall roughness, r_L
(The curves are the result from fitting eq (5.7) to the values of A_o/B_o)

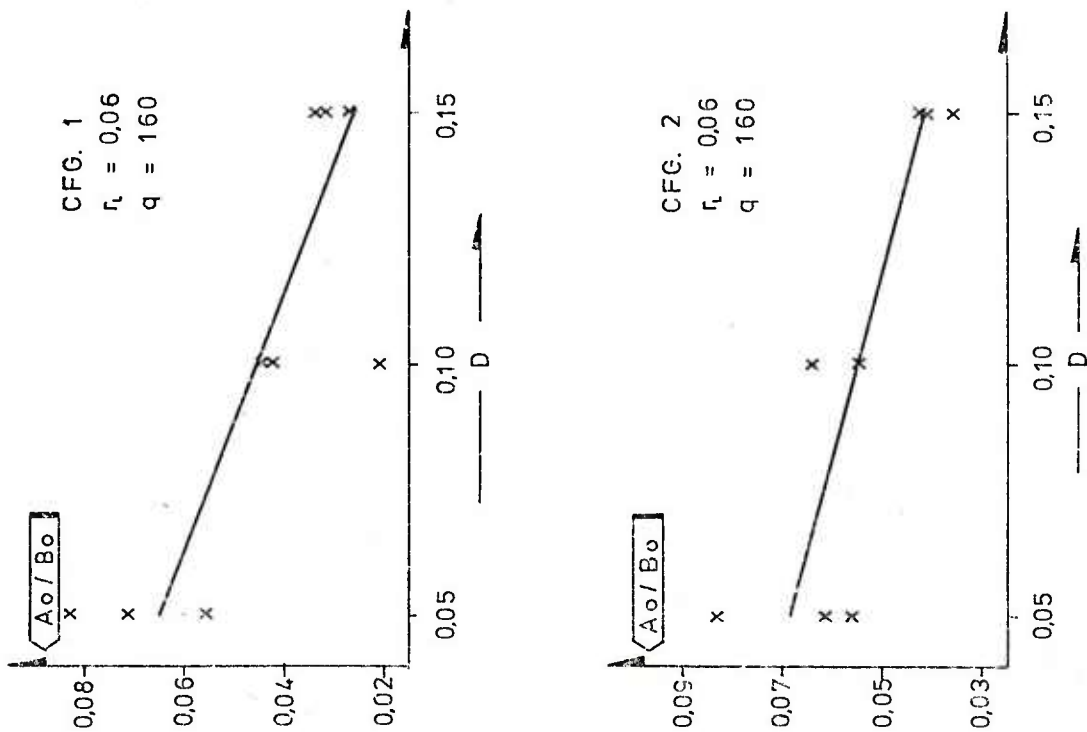


Figure 5.3 A_o/B_o as function of tube diameter, D
(The curves are the result from fitting eq (5.8) to the values of A_o/B_o)

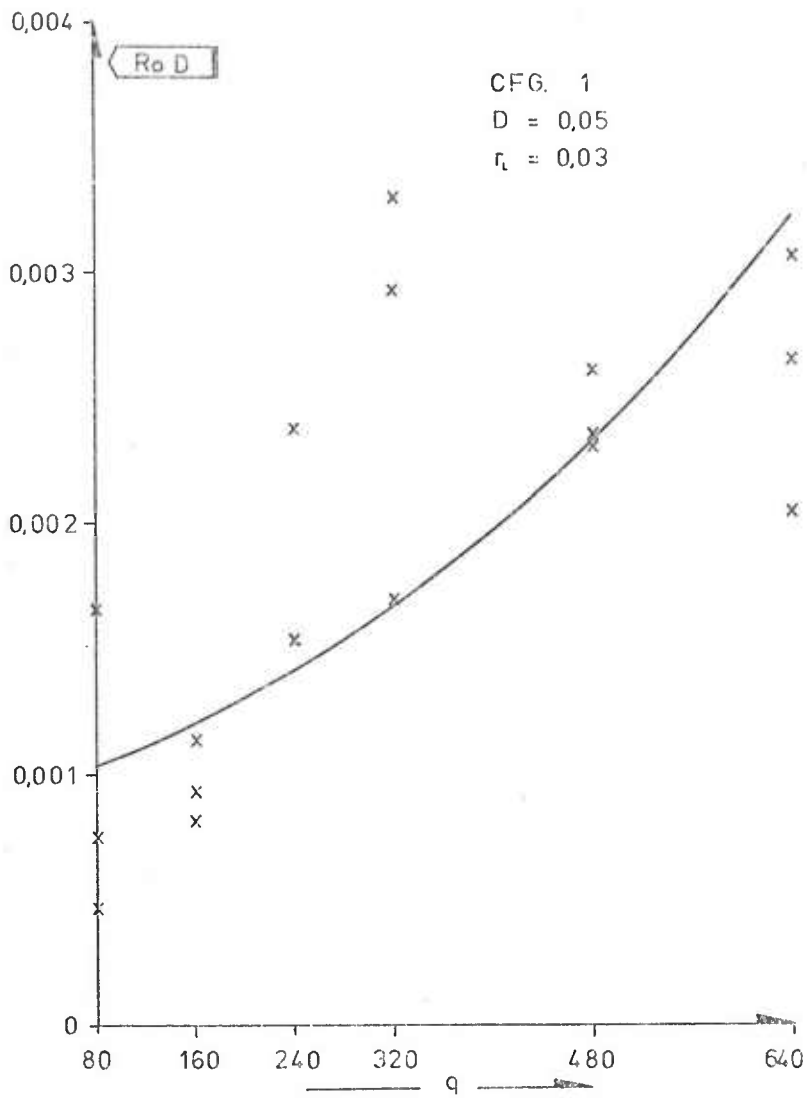


Figure 5.4 $R_0 D$ as a function of charge group, q
(The curve is the result from fitting eq (5.9) to the values of $R_0 D$)

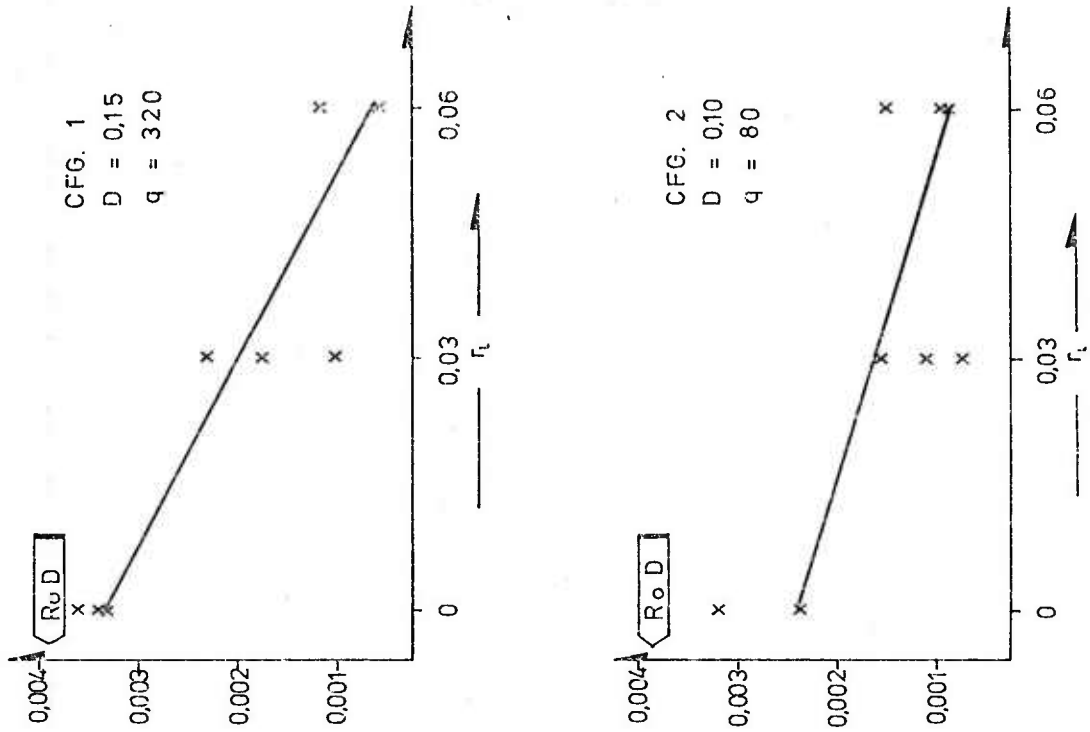


Figure 5.5 $R_o D$ as a function of wall roughness, r_L
 (The curves are the result from fitting eq (5.10) to the values of $R_o D$)

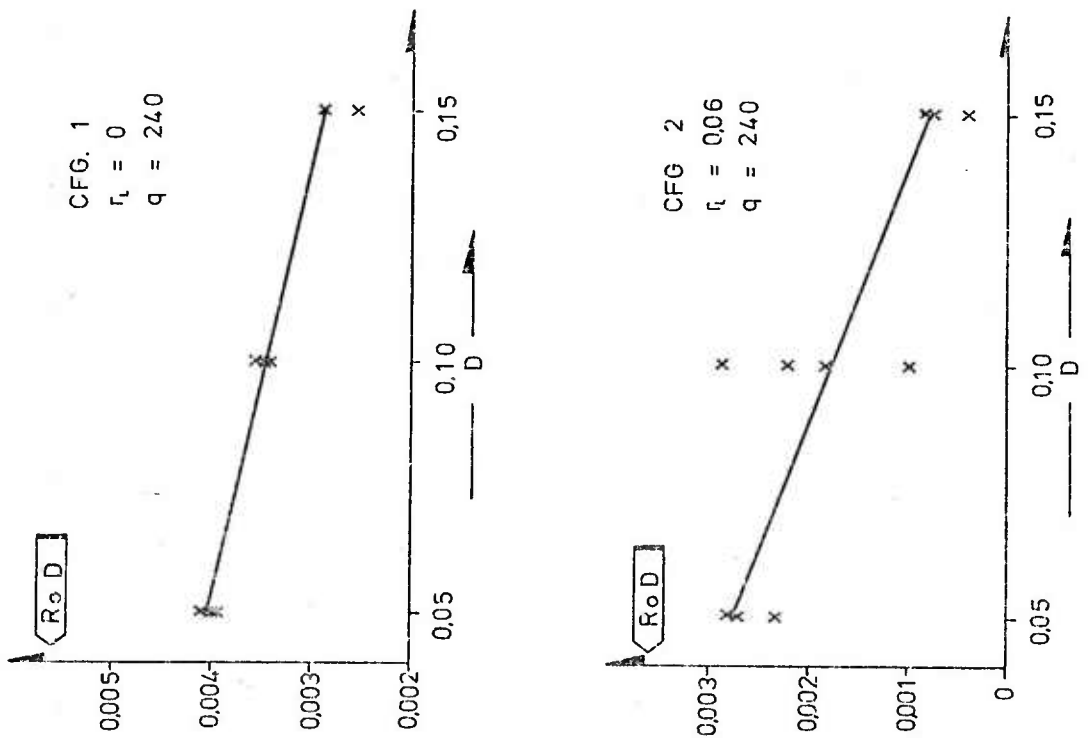


Figure 5.6 $R_o D$ as function of tube diameter, D
 (The curves are the result from fitting eq (5.11) to the values of $R_o D$)

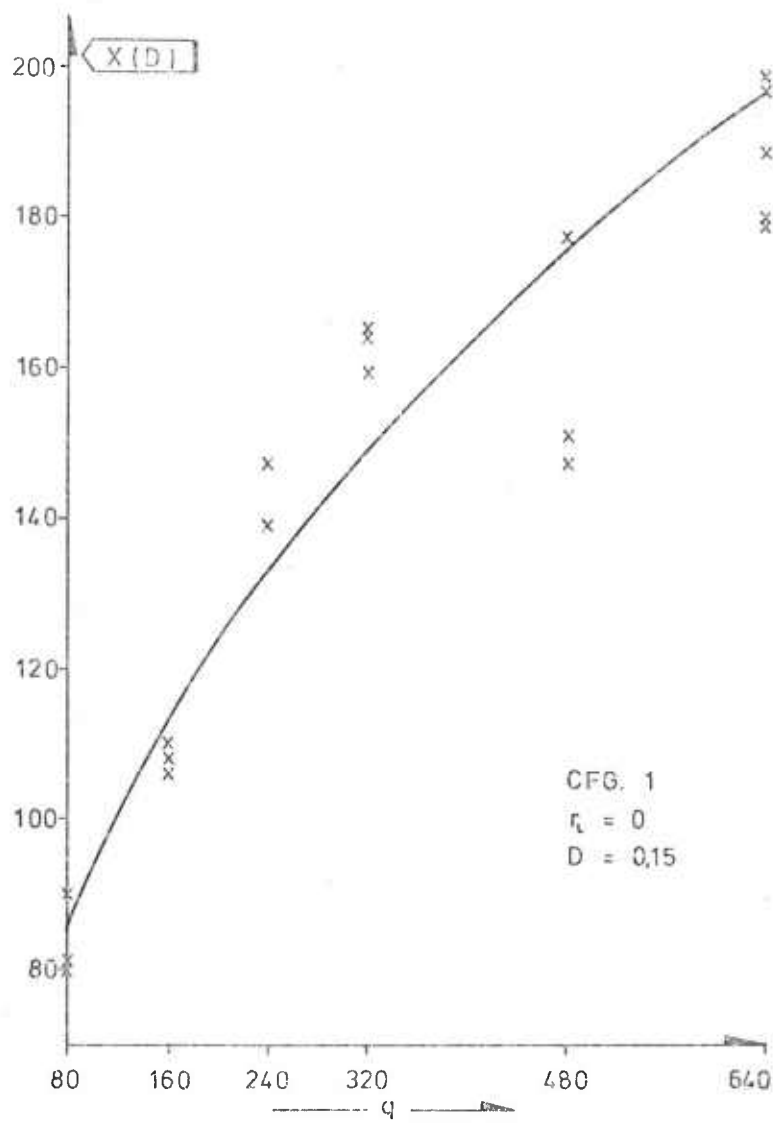


Figure 6.1 Dependence of the 50 mbar limit on charge group. 9
 (The curve is the result from fitting eq (6.2) to the values of x)

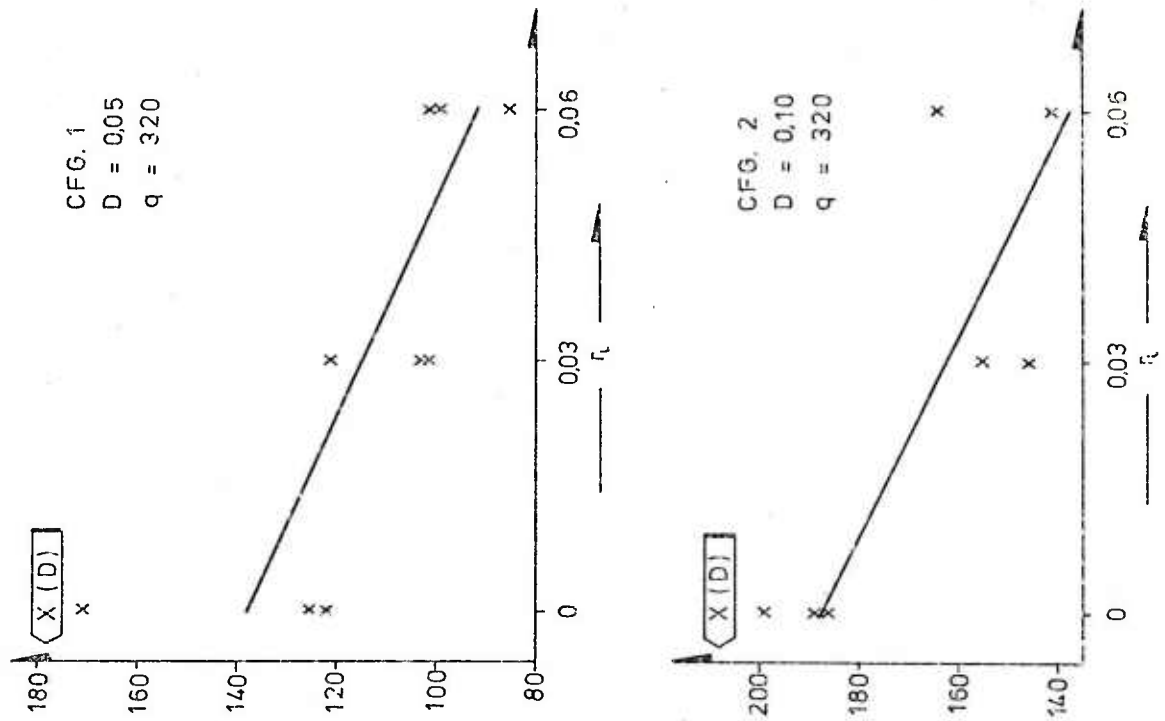


Figure 6.2 Dependence of the 50 mbar limit on wall roughness, r_L
(The curves are the result from fitting eq (6.3) to the values of x)

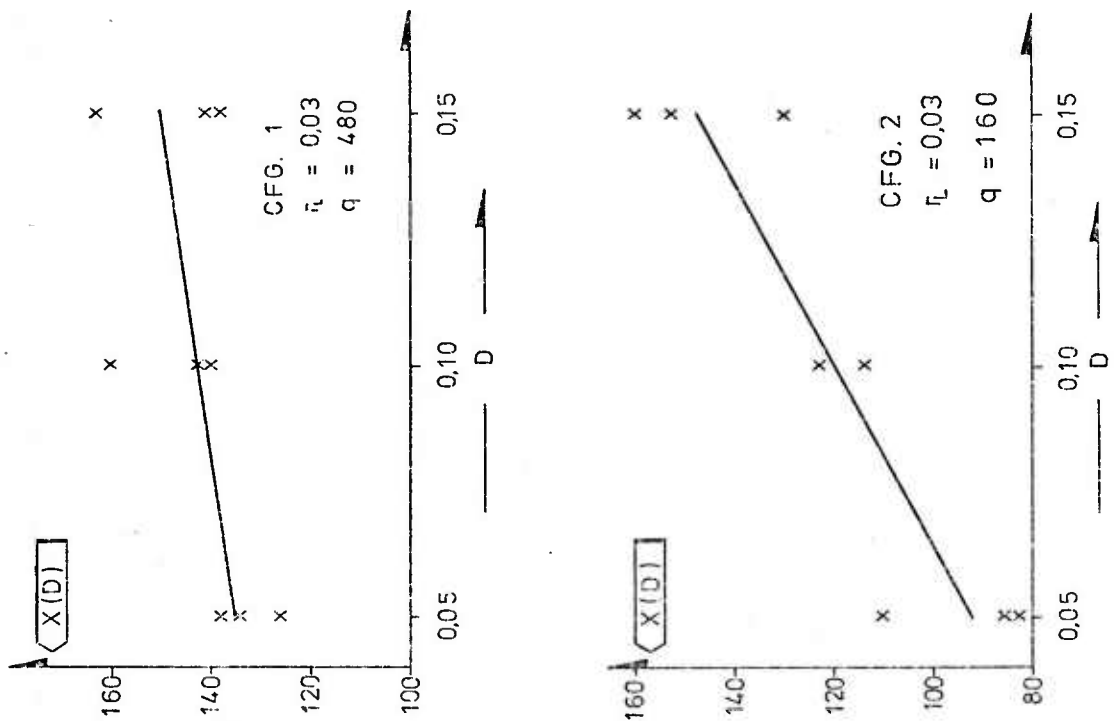


Figure 6.3 Dependence of the 50 mbar limit on tube diameter, D
(The curves are the result from fitting eq (6.4) to the values of x)

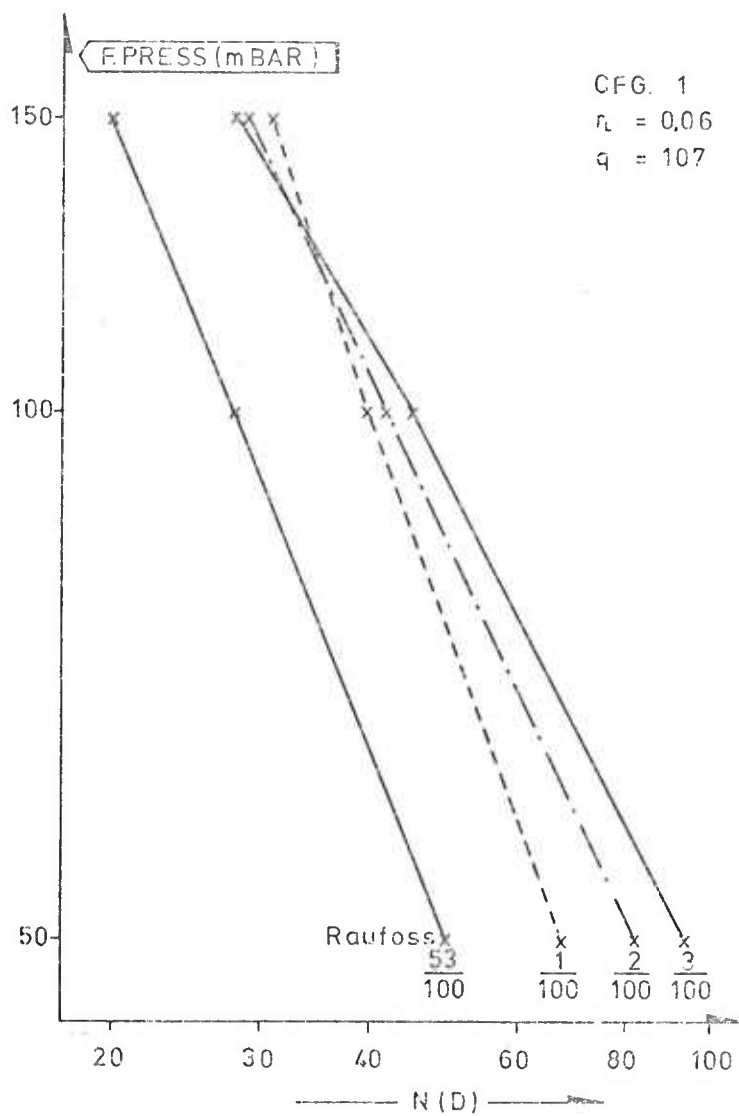


Figure 7.1 Comparison between Raufoss shot no 9 and model tests

CFG.1

D(m)	$\begin{matrix} q \text{ (kgm}^{-3}) \\ r_L \end{matrix}$	80	160	240	320	480	640
0.05	0	1.71	3.47	4.14	5.33	7.64	8.50
	0.03	0.66	1.10	1.47	1.56	2.01	2.58
	0.06		0.51	0.72	0.74	1.03	1.23
0.10	0	1.47	2.52	4.91	5.42	8.90	6.37
	0.03	0.44	1.03	1.68	1.16	1.79	2.12
	0.06	0.37	0.47	0.46	0.64	0.91	0.99
0.15	0	1.11	1.92	3.71	3.77	4.77	5.38
	0.03	0.48	0.57	0.75	0.95	1.18	1.46
	0.06	0.30	0.39	0.46	0.50	0.58	0.77

Table 3.1a Front pressure (bar) at position N = 10

CFG.2

D(m)	$\begin{matrix} q \text{ (kgm}^{-3}) \\ r_L \end{matrix}$	80	160	240	320	480	640
0.05	0	1.92	3.12	4.61	4.67	6.79	6.71
	0.03	0.41	0.90		1.56	1.97	2.05
	0.06	0.21	0.19	0.62	0.48	0.93	1.13
0.10	0	1.61	2.12	2.77	3.57	3.36	
	0.03	0.42	0.70	1.01	1.61	1.49	
	0.06	0.28	0.42	0.60	0.67	0.89	
0.15	0	1.11	1.94	2.72	3.28	4.65	
	0.03	0.43	0.63	0.77	0.83	1.01	
	0.06	0.22	0.35	0.45	0.51	0.58	

Table 3.1b Front pressure (bar) at position N = 10

CFG.1

D (m)	0.05			0.10			0.15		
r_L $q \text{ (kgm}^{-3}\text{)}$	0	0.03	0.06	0	0.03	0.06	0	0.03	0.06
80	14.81	15.83		17.36	21.45	21.40	26.14	30.12	23.69
160	13.02	12.55	17.62	15.57	18.94	21.32	25.18	25.60	26.60
240	12.27	14.01	15.47	17.08	19.01	21.17	16.05	24.90	27.53
320	10.55	14.38	15.06	16.38	18.86	21.42	15.42	24.60	28.97
480	8.78	14.65	13.75	11.20	14.63	18.79	14.65	26.03	32.52
640	7.59	11.93	13.11	10.05	14.80	18.15	12.53	22.62	26.52

Table 3.2 Values of γ

CFG.1

$$\gamma = a + bD$$

r_L	0			0.03			0.06		
$q \text{ (kgm}^{-3}\text{)}$	a	b	R	a	b	R	a	b	R
80	8.11	113.3	0.95	8.18	142.9	0.99	16.52	45.8	D = 0.05 missing
160	5.80	121.6	0.95	5.98	130.5	1.00	12.87	69.8	0.99
240	10.81	45.9	0.85	8.42	103.9	1.00	9.33	120.6	1.00
320	9.38	47.7	0.78	9.06	102.2	1.00	7.91	139.1	1.00
480	5.54	60.7	0.99	7.06	113.8	0.87	2.92	187.7	0.97
640	5.12	49.4	1.00	5.76	106.9	0.97	5.85	134.1	0.99

Table 3.3 Dependence of γ on D

$$P = P_0 \left(\frac{N}{20} \right)^{-B}$$

CFG.1		$r_L = 0$			$r_L = 0.03$			$r_L = 0.06$		
q	D	P_0	B	R	P_0	B	R	P_0	B	R
80	0.05	0.494	1.725	0.98	0.259	1.347	0.96	0.246	1.319	0.96
	0.10	0.372	1.540	0.82	0.146	0.963	0.66	0.175	1.189	0.62
	0.15	0.321	1.362	0.89	0.259	1.196	0.89	0.159	0.890	0.61
160	0.05	0.534	1.378	0.98	0.299	1.156	0.97	0.266	1.442	0.94
	0.10	0.553	1.634	0.91	0.282	1.041	0.93	0.219	1.034	0.66
	0.15	0.521	1.494	0.98	0.249	1.601	0.77	0.206	0.663	0.60
240	0.05	0.611	1.443	0.99	0.504	1.471	0.96	0.429	1.423	0.97
	0.10	0.655	1.593	0.96	0.339	1.111	0.94	0.257	1.371	0.87
	0.15	0.628	1.376	0.96	0.342	1.146	0.93	0.288	0.913	0.79
320	0.05	0.825	1.555	0.99	0.554	1.571	0.99	0.584	1.794	0.95
	0.10	0.722	1.401	0.97	0.515	1.120	0.95	0.416	1.276	0.98
	0.15	0.745	1.435	0.98	0.454	1.205	0.95	0.335	1.077	0.85
480	0.05	1.363	1.664	0.99	0.566	1.349	0.97	0.442	1.245	0.99
	0.10	0.941	1.351	0.98	0.540	1.196	0.98	0.556	1.240	0.97
	0.15	1.270	1.738	0.99	0.552	1.176	0.95	0.398	1.105	0.97
640	0.05	1.690	1.763	0.99	0.646	1.327	0.97	0.671	1.591	0.95
	0.10	1.340	1.571	0.99	0.588	1.226	0.94	0.595	1.366	0.94
	0.15	1.389	1.660	0.99	0.666	1.395	0.96			

Table 4.1a Curve fitting on front pressures obtained from arrival time measurements

$$P = P_0 \left(\frac{M}{20} \right)^{-B}$$

CFG.2		$r_L = 0$			$r_L = 0.03$			$r_L = 0.06$		
q	D	P_0	B	R	P_0	B	R	P_0	B	R
80	0.05	0.391	1.405	0.63	0.317	1.255	0.99	0.373	1.684	0.98
	0.10	0.385	1.506	0.84	0.189	1.180	0.68	0.181	1.281	0.71
	0.15	0.388	1.448	0.97	0.154	0.660	0.62	0.227	1.092	0.86
160	0.05	0.539	1.501	0.97	0.355	1.039	0.96	0.294	0.973	0.66
	0.10	0.432	1.263	0.91	0.216	0.609	0.45	0.312	1.217	0.91
	0.15	0.570	1.570	0.99	0.276	0.977	0.83	0.245	0.612	0.62
240	0.05	0.641	1.379	0.92				0.326	0.892	0.69
	0.10	0.579	1.134	0.96	0.319	0.976	0.96	0.478	1.199	0.94
	0.15	0.616	1.306	0.97	0.327	0.946	0.94	0.333	0.894	0.85
320	0.05	0.923	1.324	0.99	0.631	1.521	0.95	0.353	0.883	0.65
	0.10	0.662	1.173	0.98	0.388	1.184	0.98	0.590	1.387	0.97
	0.15	0.707	1.195	0.98	0.434	1.128	0.99	0.382	1.308	0.93
480	0.05	1.036	1.517	0.99	0.630	1.358	0.96	0.589	1.283	0.95
	0.10	1.023	1.273	0.99	0.642	1.262	0.95	0.609	1.238	0.94
	0.15	1.089	1.318	0.99	0.493	1.081	0.98	0.494	1.308	0.96
640	0.05	2.076	1.660	0.98	0.662	1.156	0.97	0.561	1.213	0.96
	0.10	1.579	1.521	1.00						
	0.15									

Table 4.1b - Curve fitting on front pressures obtained from arrival time measurements

$$P_o = ae^{bq}$$

(a)		CFG.1			(b)		
r_L	D	a	b	R	a	b	R
0	0.05	0.367	0.0026	0.99	0.322	0.0031	0.99
	0.10	0.360	0.0021	0.98	0.302	0.0026	1.00
	0.15	0.317	0.0026	0.97	0.347	0.0024	0.98
0.03	0.05	0.270	0.0016	0.87	0.302	0.0015	0.89
	0.10	0.179	0.0023	0.87	0.142	0.0031	0.99
	0.15	0.216	0.0019	0.96	0.162	0.0026	0.93
0.06	0.05	0.243	0.0016	0.85	0.277	0.0011	0.83
	0.10	0.157	0.0024	0.96	0.186	0.0030	0.89
	0.15	0.146	0.0024	0.96	0.191	0.0020	0.98

Table 4.2 Dependence of P_o on q

$$B = b_1 + b_2 D + b_3 r_L$$

CFG.1

(a)	i	1	2	3
	b_i	1.75	-2.70	-5.39
	R_i		0.68	0.75

CFG.2

(b)	i	1	2	3
	b_i	1.52	-2.01	-4.26
	R_i		0.60	0.68

Table 4.3 Dependence of B on D and r_L

CFG.1

 $D = 0.65 \quad r_L = 0$

$\begin{matrix} q \\ N \end{matrix}$	80	160	240	320	480	640
20.8	0.297	0.267	0.521	0.538	0.898	1.351
30.8	0.139	0.165	0.228	0.224	0.481	0.604
40.8	0.089	0.120	0.133	0.167	0.279	0.402
50.8	0.055	0.088	0.086	0.082		0.252
70.9	0.017	0.045	0.060	0.076	0.105	0.126
80.9	0.032					
90.0		0.039	0.047	0.055	0.082	0.096
101.0	0.019					
111.0		0.023	0.028	0.033	0.055	0.058
119.0	0.017					
131.0		0.012	0.025	0.021	0.043	0.049
141.0	0.021			0.018	0.040	0.054
161.0	0.021	0.023	0.031	0.036	0.054	0.057

$$P = P_0 \left(\frac{N}{20} \right)^{-R}$$

P_0	0.227	0.306	0.419	0.466	0.851	1.245
B	1.375	1.446	1.453	1.510	1.504	1.656
R	0.93	0.97	0.93	0.97	0.99	0.99

Table 4.4a Measured front pressures (bar) and results from fitting of eq (4.1) to these pressures

CFG.1

 $D = 0.10 \quad r_L = 0$

$\begin{matrix} q \\ N \end{matrix}$	80	160	240	320	480	640
20.4	0.256	0.378	0.418	0.530	0.772	0.968
25.4	0.196	0.289	0.298			0.565
29.4	0.124	0.148	0.221	0.268	0.353	0.752
35.45	0.114	0.165	0.177			
40.45	0.078	0.127	0.175	0.175	0.304	0.259
44.5	0.079	0.114				
50.5	0.057	0.062	0.074	0.112	0.135	0.176
59.5	0.044	0.059	0.082	0.132	0.181	0.179
70.5	0.030	0.036	0.043	0.064	0.078	0.088
80.5	0.026	0.033	0.044	0.076	0.093	0.093
89.9			0.042	0.052	0.066	0.092
99.0			0.032	0.038	0.054	0.053
109.9				0.038	0.050	0.055
119.9				0.031	0.041	0.043
129.9					0.028	0.034
139.9				0.025	0.031	0.033
149.9					0.026	0.030
159.9					0.032	
169.9					0.025	0.030

$$P = P_0 \left(\frac{N}{20} \right)^{-B}$$

P_0	0.270	0.401	0.440	0.549	0.774	1.068
B	1.666	1.811	1.642	1.579	1.636	1.733
R	0.99	0.98	0.98	0.99	0.99	0.99

Table 4.4b Measured front pressures (bar) and results from fitting of eq (4.1) to these pressures

CFG.1

 $D = 0.15 \quad r_L = 0$

$\frac{q}{N}$	80	160	240	320	480	640
20.1	0.259	0.408	0.536	0.638	0.737	
23.93	0.181	0.250	0.312			0.752
26.77	0.153	0.219	0.242	0.320	0.436	0.634
33.93	0.078	0.136	0.182	0.226	0.353	0.445
40.13	0.075	0.081	0.130	0.188	0.255	
46.8		0.077	0.091	0.145		0.208
54.03	0.028	0.037	0.076	0.102	0.113	
58.17						0.114
66.4	0.053	0.064	0.087	0.082	0.121	
73.07						0.127
79.73	0.030	0.040	0.050	0.062	0.067	
86.4						0.062
93.03			0.033	0.041	0.051	
99.7						0.053
106.33					0.063	
112.97						0.063

$$P = P_0 \left(\frac{N}{20} \right)^{-B}$$

P_0	0.225	0.338	0.419	0.583	0.735	0.998
B	1.551	1.691	1.694	1.681	1.625	1.730
R	0.94	0.95	0.98	1.00	0.98	0.98

Table 4.4c Measured front pressures (bar) and results from fitting of eq (4.1) to these pressures

		$r_L = 0$						$r_L = 0.03$						$r_L = 0.06$					
y	NO	A_0	B_0	$D_0 \times 10^3$	$S \times 10^4$	$\frac{S}{S_1+S_2}$	NO	A_0	B_0	$D_0 \times 10^3$	$S \times 10^4$	$\frac{S}{S_1+S_2}$	NO	A_0	B_0	$D_0 \times 10^3$	$S \times 10^4$	$\frac{S}{S_1+S_2}$	
80	210	0.0608	0.864	-0.779	0.725	2.42	256	0.0836	3.088	-0.383	0.238	2.99	296	0.0386	0.565	-0.227	0.498	70.85	
	211	0.0669	0.911	-0.470	0.333	2.06	257	0.0672	2.108	-0.568	1.348	3.35	297	0.0594	1.771	-1.294	3.602	2.33	
	212	0.0735	1.012	-0.936	0.937	1.19	258	0.0421	1.126	-0.783	1.732	5.25	299	0.0621	1.607	-0.966	1.313	7.44	
160	213	0.1045	1.314	0.861	1.163	1.75	259	0.0872	1.953	0.114	0.578	1.46	301	0.0717	1.294	-0.893	1.630	5.58	
	214	0.1059	1.262	-0.927	1.209	1.63	260	0.0937	2.403	0.125	0.372	1.32	302	0.0629	0.732	-1.041	5.626	4.62	
	215	0.1276	2.106	0.628	0.326	2.52	261	0.0947	2.250	-1.147	1.598	2.73	303	0.0499	0.599	-2.321	14.246	12.22	
240	216	0.0945	1.095	0.792	0.271	2.46	263	0.0866	1.349	-0.235	0.373	1.39	304	0.0655	0.785	-3.543	25.393	1.99	
	217	0.1203	1.232	-0.591	0.664	2.51	264	0.0996	1.797	-0.860	1.100	2.74	305	0.0905	1.733	-1.235	0.959	2.68	
	218	0.1126	1.176	-0.590	0.864	2.71							306	0.0915	1.525	-1.588	4.466	3.13	
320	219	0.1077	0.668	-3.068	6.165	6.03	265	0.0910	1.174	-0.069	0.571	1.18	307	0.0893	1.418	-1.024	2.913	2.62	
	220	0.1083	1.067	-1.329	0.584	2.14	266	0.0901	1.240	-0.674	1.040	2.36	308	0.0909	1.485	-2.174	1.677	0.64	
	221	0.1600	1.529	0.433	0.396	1.35	267	0.1141	1.834	-0.563	1.366	3.14	309	0.0696	0.631	-1.788	4.045	6.01	
480	222	0.1454	0.634	-2.511	3.504	2.30	268	0.1154	1.488	-0.154	0.179	1.29	310	0.1194	2.037	-0.513	0.306	1.64	
	223	0.1563	0.766	-2.325	2.131	2.21	269	0.1293	1.674	0.169	0.441	1.79	311	0.1127	1.734	-1.329	0.583	10.11	
	224	0.1649	1.006	-1.652	1.181	3.61	270	0.1244	1.629	0.395	0.415	2.47	312	0.1197	2.132	-1.219	1.417	2.27	
640	226	0.1766	0.949	-1.219	2.111	3.36	271	0.1415	1.633	-0.210	0.467	1.90	313	0.1166	1.675	-1.098	1.745	1.42	
	227	0.1630	0.676	-1.152	0.830	10.22	272	0.1599	1.979	0.377	0.632	1.65	314	0.1224	1.251	-3.678	4.540	18.85	
							273	0.1296	1.453	0.179	0.617	1.65	315	0.0982	1.023	-3.311	5.997	7.06	

Table 5.1a Results from fitting of eq (5.2) to the measured arrival times

2:100 CFG.1

q	$r_L = 0$						$r_L = 0.03$						$r_L = 0.06$					
	NO	A_0	B_0	$D_0 \times 10^3$	$S \times 10^4$	$\frac{S}{S_1+S_2}$	NO	A_0	B_0	$D_0 \times 10^3$	$S \times 10^4$	$\frac{S}{S_1+S_2}$	NO	A_0	B_0	$D_0 \times 10^3$	$S \times 10^4$	$\frac{S}{S_1+S_2}$
80	335	0.1408	2.393	-0.962	4.620	1.64	372	0.0886	3.472	0.215	1.350	1.37	415	0.1827	7.864	1.165	2.057	1.28
	336	0.1427	2.231	-0.066	4.947	1.58												
	337	0.1535	2.876	1.266	3.089	1.62	373	0.0972	4.142	0.152	1.709	1.74	416	0.1263	4.674	-0.478	2.983	1.40
	338	0.1576	2.899	1.185	3.257	1.15												
	339	0.1496	2.671	1.104	2.486	1.21	374	0.1948	7.105	-2.340	3.051	1.99	417	0.1370	4.425	-0.112	3.478	1.52
	340	0.1409	2.318	-0.100	2.219	1.13												
100	341	0.1444	2.484	0.017	2.317	1.67												
	342	0.1274	2.076	-0.841	3.116	2.09												
	343	0.1622	1.905	-0.576	2.690	1.61	375	0.3093	7.810	6.473	2.195	1.53	419	0.1592	3.760	-2.957	5.432	1.56
	344	0.1693	1.824	-2.416	3.444	2.62	377	0.2212	5.650	3.854	2.624	1.72	420	0.1919	9.378	5.485	2.468	1.44
	345	0.1785	2.244	0.766	1.937	1.78	378	0.1903	4.581	3.838	3.030	2.88	421	0.2127	4.784	-6.327	7.007	1.85
	346	0.1763	2.155	-0.402	2.249	1.82												
200	347	0.2246	2.512	-3.667	4.979	2.10	379	0.1845	3.482	3.232	2.179	1.13	422	0.2155	3.065	-12.222	229.27	1.36
	348	0.2258	2.543	-1.841	3.721	2.02	380	0.2338	6.882	6.905	3.584	1.81						
	349	0.2327	2.567	-0.838	3.047	1.94	381	0.3228	5.976	-0.166	9.432	4.85						
	350	0.2907	3.365	0.302	2.096	1.20	382	0.1944	2.804	0.746	2.801	1.23	425	0.2561	3.244	-4.225	5.495	5.24
	351	0.2641	2.313	0.059	1.453	1.21	384	0.3220	4.729	-3.716	10.192	7.89	426	0.2235	3.238	-5.999	6.201	2.39
	352	0.3024	2.955	1.032	1.923	1.32												
400	353	0.3278	2.057	-7.388	8.713	2.28	385	0.2677	3.644	9.878	6.280	6.31	428	0.2817	3.400	-8.098	12.117	13.54
	354	0.3895	3.016	-7.854	10.398	2.23	387	0.3049	3.965	5.485	2.256	1.64	429	0.2877	3.672	-9.959	13.131	7.29
	355	0.3346	2.194	-3.085	4.194	1.32	388	0.2693	4.326	11.368	6.607	6.90	430	0.2814	4.305	-4.686	7.220	2.07
	356	0.3208	1.391	-9.063	19.549	4.22												
	357	0.3645	1.605	-6.257	8.514	1.82												

Table 5.1b Results from fitting of eq (5.2) to the measured arrival times

q	$r_L = 0$						$r_L = 0.03$						$r_L = 0.06$					
	NO	A_u	R_u	D_u $\times 10^3$	S $\times 10^4$	$\frac{S}{S_1+S_2}$	NO	A_0	B_0	D_0 $\times 10^3$	S $\times 10^4$	$\frac{S}{S_1+S_2}$	NO	A_0	B_0	D_0 $\times 10^3$	S $\times 10^4$	$\frac{S}{S_1+S_2}$
80	450	0.2146	4.475	3.748	2.319	1.16	465	0.2439	6.333	5.708	2.019	2.27	477	0.1537	5.096	3.572	1.263	1.99
	451	0.2352	3.883	2.845	1.578	1.27	466	0.2531	7.484	6.652	2.663	191.69	478	0.2213	9.196	2.523	1.419	1.24
	452	0.2096	3.817	2.195	6.054	1.14	467	0.2413	7.776	6.601	2.453	*	479	0.2994	13.321	3.719	1.516	1.51
	453	0.2035	3.493	3.907	2.352	1.32												
160	454	0.2828	3.646	2.934	2.242	1.18	468	0.3309	8.924	6.197	2.773	*	480	0.4641	14.495	8.269	3.968	3.67
	455	0.2975	4.099	0.174	1.622	2.64	469	0.2695	6.695	5.512	2.358	1.69	481	0.4893	17.965	10.014	5.162	3.56
240	456	0.2897	3.737	-0.212	1.632	1.34	470	0.2541	6.279	5.207	2.471	1.62	482	0.3516	11.461	4.390	2.419	1.31
	457	0.4123	4.995	1.298	2.573	1.46	471	0.3085	5.920	3.202	1.955	1.11	483	0.5711	16.290	9.719	5.728	4.19
320	458	0.3852	4.482	0.070	1.400	1.65	472	0.3050	6.313	4.630	1.467	1.62	484	0.3731	7.925	2.007	3.553	1.58
							473	0.3470	7.568	7.403	2.631	2.26	485	0.6054	10.715	6.961	3.131	2.13
	460	0.4585	4.598	-0.470	3.332	1.27	474	0.3195	5.216	2.806	1.660	4.84	486	0.4555	10.249	5.364	3.379	2.65
	461	0.4529	4.543	2.451	3.047	1.37	475	0.4416	8.683	3.033	8.402	4.80	487	0.2871	6.018	3.055	2.855	1.25
400	462	0.4413	4.280	1.631	3.033	1.07	476	0.3018	4.437	2.722	1.510	6.31						
	463	0.4164	3.767	-3.352	3.106	1.64	488	0.4692	6.315	7.928	8.567	4.59	502	0.4277	5.111	-18.445	10.382	7.51
	464	0.4006	3.520	-4.594	5.387	2.13	489	0.3894	5.364	8.428	3.010	*	503	0.4720	6.667	-5.465	7.034	3.19
	469	0.4792	2.704	-10.770	18.235	6.06	497	0.5001	5.573	7.148	6.424	*						
640	490	0.4699	3.187	-6.228	28.204	2.34	498	0.4361	4.686	6.391	3.556	*	504	0.4848	7.397	-4.671	5.454	4.59
	491	0.4927	2.945	-11.677	26.348	4.59	499	0.4254	5.083	12.318	16.105	21.30	505	0.5166	10.598	-3.085	10.416	6.89
	492	0.5326	2.212	-12.824	27.394	10.05	500	0.4479	5.891	12.173	12.816	26.22		9.5443	9.150	-0.207	4.966	3.54
	493	0.5695	2.046	-17.326	26.584	7.91												
	494	0.5415	2.522	-3.464	29.375	3.82												

Table 5.1c - Results from fitting of eq (5.2) to the measured arrival times

*Too few points

q	$r_L = 0$						$r_L = 0.03$						$r_L = 0.06$					
	NO	A_0	B_0	$D_0 \times 10^3$	$S \times 10^4$	$\frac{S}{S_1 + S_2}$	NO	A_0	B_0	$D_0 \times 10^3$	$S \times 10^4$	$\frac{S}{S_1 + S_2}$	NO	A_0	B_0	$D_0 \times 10^3$	$S \times 10^4$	$\frac{S}{S_1 + S_2}$
80	238	0.0749	1.071	-1.620	2.345	4.35	287	0.0623	1.178	-1.849	5.994	10.33	317	0.0790	1.756	-0.789	1.011	20.12
	239	0.0647	0.965	-1.167	4.062	1.78	288	0.0520	0.992	-1.273	5.030	5.95	318	0.0474	0.784	-0.436	0.123	5.07
	240	0.0696	0.945	-0.885	3.053	1.99												
160	241	0.0903	1.403	1.394	1.392	5.26	289	0.0975	1.700	-2.633	7.453	3.30	319	0.0585	0.821	-4.287	15.150	3.79
	242	0.0868	0.861	-0.858	1.783	1.56	290	0.1031	2.014	-2.603	6.967	2.64	321	0.0743	1.216	-1.290	2.322	2.21
	243	0.1089	1.535	0.812	1.757	1.57							322	0.1029	1.331	-0.215	1.125	3.89
240	244	0.1141	1.243	0.684	1.231	1.06	281	0.0639	1.366	-0.940	3.689	1.55	323	0.0994	1.463	-5.649	12.043	3.27
	245	0.1663	1.890	-3.124	15.874	1.44							324	0.1002	1.354	-3.071	7.254	3.22
	246	0.1317	1.360	-1.674	6.292	7.63							325	0.0897	1.267	0.164	1.076	2.03
320	248	0.1059	1.285	-2.360	2.790	9.43	283	0.1272	1.959	-2.886	6.791	3.36	326	0.1097	1.470	-1.605	1.540	13.59
	249	0.2313	2.126	-3.919	2.219	2.31	284	0.1097	1.285	0.718	3.319	1.79	327	0.1004	1.234	-1.816	5.359	2.08
							285	0.0994	1.694	-2.321	3.345	1.21	328	0.0883	0.914	-2.841	5.079	3.48
480	250	0.2036	1.036	-1.656	3.679	26.67	286	0.1690	2.512	-2.134	2.882	3.62	329	0.1505	1.783	-3.472	1.783	2.68
	251	0.2141	1.116	-2.621	3.923	1.61	291	0.1159	1.134	1.266	3.213	2.19	330	0.1377	2.091	-1.738	5.527	1.71
	252	0.2194	1.126	-4.479	12.301	6.09	292	0.1477	2.093	-1.579	3.933	2.10	331	0.1507	1.829	-2.706	2.042	2.72
640	254	0.2574	1.168	-1.379	2.170	9.19	293	0.2047	2.699	0.247	1.749	1.52	332	0.1837	2.523	-2.380	5.937	3.53
	255	0.1398	0.591	1.095	5.000	1.95	294	0.2010	2.413	-1.798	2.024	5.13	333	0.1430	1.701	-0.845	0.761	17.52
							295	0.1720	2.032	-0.994	2.273	2.28	334	0.1373	1.648	-5.590	10.071	8.49

Table 5.1d Results from fitting of eq (5.2) to the measured arrival times

q	$r_L = 0$						$r_L = 0.03$						$r_L = 0.06$					
	NO	A_0	B_0	$D_0 \times 10^3$	$S \times 10^4$	$\frac{S}{S_1 + S_2}$	NO	A_0	B_0	$D_0 \times 10^3$	$S \times 10^4$	$\frac{S}{S_1 + S_2}$	NO	A_0	B_0	$D_0 \times 10^3$	$S \times 10^4$	$\frac{S}{S_1 + S_2}$
80	358	0.1417	2.110	0.476	2.641	1.46	389	0.0866	2.108	-1.168	4.061	1.94	402	0.0764	2.873	0.832	2.022	1.35
	371	0.1549	2.553	0.953	2.235	1.59	396	0.0834	3.390	1.202	1.657	1.64	403	0.0474	1.791	0.689	2.394	1.56
							391	0.1945	4.220	-4.245	3.046	2.31	404	0.1563	4.183	-4.959	4.522	1.78
160	362	0.1799	2.033	-1.607	2.361	2.54	392	0.4976	11.809	3.330	3.855	1.07	405	0.2160	3.957	6.312	6.616	2.09
	363	0.2585	5.061	3.015	7.560	3.77	393	0.1679	6.503	-4.056	4.673	1.32	407	0.2298	3.601	-13.580	12.349	3.17
240	364	0.3612	4.316	3.140	5.246	4.29	396	0.4008	10.831	12.343	6.848	3.13	408	0.2441	3.320	-8.843	12.965	2.99
	365	0.3099	3.446	2.069	5.349	2.87	398	0.3364	7.122	2.522	3.575	4.39	409	0.2750	3.097	-12.110	13.099	3.12
	366	0.3145	4.114	1.845	1.306	4.18		0.2454	5.922	-12.725	25.201	8.72	410	0.2689	3.823	-5.960	5.345	5.38
320	367	0.3540	3.577	-0.994	4.721	1.88	399	0.3251	7.667	13.265	9.139	11.08	412	0.2299	3.914	-8.502	9.884	3.67
	368	0.3873	4.560	1.382	2.273	1.13	401	0.2914	5.572	4.045	3.539	1.87	413	0.2549	2.271	-5.925	12.196	4.54
	369	0.3632	4.051	3.197	5.056	3.66							414	0.2470	2.815	-4.403	6.653	2.21

Table 5.1e Results from fitting of eq (5.2) to the measured arrival times

$r_L = 0$							$r_L = 0.03$					$r_L = 0.06$						
q	NO	A_0	B_0	$D_0 \times 10^3$	$S \times 10^4$	$\frac{S}{S_1 + S_2}$	NO	A_0	B_0	$D_0 \times 10^3$	$S \times 10^4$	$\frac{S}{S_1 + S_2}$	NO	A_0	B_0	$D_0 \times 10^3$	$S \times 10^4$	$\frac{S}{S_1 + S_2}$
30	531	0.2718	5.267	2.997	2.397	2.58							508	0.2990	9.177	-6.221	5.595	2.37
	532	0.2253	3.547	0.483	0.992	1.24							509	0.2601	7.330	-2.266	1.480	1.93
	533	0.2137	3.619	0.395	0.899	1.12												
100	535	0.2802	3.520	0.604	0.915	1.23	522	0.3313	8.948	6.380	3.257	1.68	510	0.4791	11.321	-6.503	7.267	4.62
	536	0.2790	3.303	1.864	1.254	2.51	523	0.4397	12.515	9.567	3.863	1.90	511	0.4114	11.480	-0.901	2.409	1.63
	537	0.2742	3.071	0.654	1.182	1.40	524	0.3330	8.491	6.855	3.320	1.76	512	0.5066	12.362	-4.744	7.729	3.60
240	538	0.3900	4.209	5.784	4.748	12.77	525	0.4509	11.050	6.550	3.858	5.54	513	0.4847	9.283	-8.091	7.879	7.69
	539	0.4042	4.839	7.752	10.526	8.65	527	0.4574	11.469	5.896	3.041	3.02	514	0.6074	16.244	-2.624	8.366	4.20
	540	0.3997	4.731	7.223	10.662	10.21							515	0.5131	10.094	-8.601	7.298	9.80
320	541	0.6168	6.836	4.555	10.659	3.67	528	0.4531	9.337	7.631	5.159	6.01	516	0.5624	11.651	-6.157	8.887	1.62
	542	0.5386	6.141	10.884	11.840	6.43	529	0.4243	8.316	0.711	1.290	428.1	517	0.3667	6.694	-5.773	5.354	2.83
	543	0.6069	7.116	7.189	14.758	5.05	530	0.5012	9.908	-3.136	2.928	15.32	518	0.7072	14.683	-6.412	11.462	2.43
480	544	0.7449	5.765	-3.196	7.789	5.04	548	0.5551	9.909	5.129	6.250	5.32	552	0.5091	7.594	-17.774	23.937	11.57
	545	0.7431	5.655	-9.767	18.726	10.27	549	0.5832	9.960	3.077	6.215	1.11	553	0.4645	7.426	-8.583	14.622	12.60
	546	0.6971	5.246	-8.215	10.684	14.12	550	0.6827	11.739	-2.213	4.316	3.98	554	0.4825	10.173	-4.165	7.224	3.20

Table 5.1f Results from fitting of eq (5.2) to the measured arrival times

CFG.1

$$\frac{A_0}{B_0} = a e^{bq}$$

r_L	D (m)	a	b	R
0	0.05	0.0530	0.00259	0.96
	0.10	0.0514	0.00223	0.97
	0.15	0.0493	0.00218	0.95
0.03	0.05	0.0337	0.00167	0.90
	0.10	0.0244	0.00248	0.89
	0.15	0.0317	0.00165	0.95
0.06	0.05	0.0508	0.00076	0.50
	0.10	0.0237	0.00271	0.83
	0.15	0.0247	0.00163	0.89

Table 5.2a Dependence of A_0/B_0 on q

CFG.2

$$\frac{A_0}{B_0} = a e^{bq}$$

r_L	D (m)	a	b	R
0	0.05	0.0539	0.00254	0.97
	0.10	0.0550	0.00160	0.71
	0.15	0.0552	0.00176	0.92
0.03	0.05	0.0502	0.00081	0.72
	0.10	0.0284	0.00155	0.57
	0.15	0.0299	0.00142	0.96
0.06	0.05	0.0597	0.00056	0.57
	0.10	0.0249	0.00400	0.64
	0.15	0.0328	0.00131	0.84

Table 5.2b Dependence on A_0/B_0 on q

$$\frac{A_0}{B_0} = a + b r_L$$

CF5.1

D(m)	q (kgm ⁻³)	a	b	R
0.05	80	0.0648	-0.576	0.53
	160	0.0645	-0.076	0.11
	240	0.0884	-0.466	0.70
	320	0.1125	-0.782	0.63
	480	0.1816	-2.320	0.89
	640	0.2279	-2.819	0.82
0.10	80	0.0560	-0.588	0.89
	160	0.0794	-0.847	0.88
	240	0.0811	-0.590	0.60
	320	0.0971	-0.497	0.74
	480	0.1327	-1.174	0.80
	640			
0.15	80	0.0538	-0.500	0.93
	160	0.0711	-0.751	0.93
	240	0.0787	-0.715	0.91
	320	0.0935	-0.988	0.96
	480	0.1251	-1.153	0.74
	640	0.1944	-2.511	0.88

Table 5.3a Dependence of A_0/B_0 on r_L

$$\frac{A_0}{B_0} = a + b r_L$$

CF5.2

D(m)	q (kgm ⁻³)	a	b	R
0.05	80	0.0694	-0.301	0.81
	160	0.0753	-0.219	0.38
	240	0.0872	-0.355	0.51
	320	0.1342	-0.496	0.53
	480	0.1771	-1.975	0.86
	640	0.2267	-2.926	0.80
0.10	80	0.0581	-0.531	0.81
	160	0.0596	-0.177	0.22
	240	0.0743	-0.138	0.21
	320	0.0815	-0.169	0.19
	480			
	640			
0.15	80	0.0582	-0.403	0.95
	160	0.0762	-0.747	0.83
	240	0.0800	-0.637	0.80
	320	0.0811	-0.591	0.82
	480	0.1187	-1.203	0.85
	640			

Table 5.3b Dependence of A_0/B_0 on r_L

$$\frac{A_0}{B_0} = a + bD$$

CFG.2

r_L	$q \text{ (kgm}^{-3}\text{)}$	a	b	R
0	80	0.0762	-0.120	0.82
	160	0.0748	0.044	0.14
	240	0.0929	-0.054	0.38
	320	0.1280	-0.294	0.80
	480	0.2284	-0.646	1.00
0.03	80	0.0010	-0.465	0.83
	160	0.0561	-0.158	0.68
	240	0.0487	-0.057	0.61
	320	0.0762	-0.195	0.68
	480	0.0913	-0.225	0.71
0.06	80	0.9562	-0.185	0.64
	160	0.0321	-0.273	0.82
	240	0.0800	-0.119	0.45
	320	0.1045	-0.320	0.64
	480	0.0868	-0.185	0.74

Table 5.4b Dependence of A_0/B_0 on D

$$\frac{A_0}{B_0} = a + bD$$

CFG.1

r_L	$q \text{ (kgm}^{-3}\text{)}$	a	b	R
0	80	0.0767	-0.158	0.77
	160	0.0779	0.012	0.06
	240	0.0974	-0.082	0.73
	320	0.1278	-0.194	0.40
	480	0.2249	-0.652	0.70
0.03	80	0.0292	0.017	0.14
	160	0.0431	-0.023	0.56
	240	0.0615	-0.100	0.48
	320	0.0762	-0.005	0.61
	480	0.0777	-0.041	0.38
0.06	80	0.0861	-0.011	0.10
	160	0.0475	-0.162	0.48
	240	0.0849	-0.393	0.81
	320	0.0921	-0.282	0.65
	480	0.0579	0.109	0.38
0.06	80	0.1010	-0.266	0.82

Table 5.4a Dependence of A_0/B_0 on D

CFG.1 $DR_0 = a e^{bq}$

r_L	D(m)	a	b	R
0	0.05	0.00194	0.00361	0.85
	0.10	0.00209	0.00260	0.87
	0.15	0.00157	0.00300	0.92
0.03	0.05	0.00087	0.00205	0.72
	0.10	0.00043	0.00323	0.79
	0.15	0.00061	0.00250	0.85
0.06	0.05	0.00259	0.00003	0.81
	0.10	0.00041	0.00384	0.73
	0.15	0.00033	0.00216	0.67

Table 5.5a Dependence of DR_0 on q

CFG.2 $DR_0 = a e^{bq}$

r_L	D(m)	a	b	R
0	0.05	0.00293	0.00293	0.82
	0.10	0.00262	-0.00066	0.16
	0.15	0.00245	0.00049	0.23
0.03	0.05	0.00212	-0.00022	0.12
	0.10	0.00091	-0.00179	0.34
	0.15	0.00046	0.00134	0.70
0.06	0.05	0.00291	-0.00045	0.21
	0.10	0.00087	0.00311	0.59
	0.15	0.00044	0.00171	0.58

Table 5.5b Dependence of DR_0 on q

CFG.1 $DR_0 = a + br_L$

D(m)	$q \text{ (kgm}^{-3}\text{)}$	a	b	R
0.05	80	0.00311	-0.0201	0.27
	160	0.00171	0.0342	0.43
	240	0.00362	-0.0177	0.35
	320	0.00586	-0.0412	0.37
	400	0.01153	-0.1941	0.82
	640	0.01612	-0.2580	0.80
0.10	80	0.00226	-0.0344	0.57
	160	0.00375	-0.0603	0.85
	240	0.00302	-0.0362	0.53
	320	0.00343	-0.0250	0.60
	400	0.00351	-0.0710	0.77
	640			
0.15	80	0.00199	-0.0281	0.88
	160	0.00271	-0.0442	0.93
	240	0.00248	-0.0344	0.93
	320	0.00331	-0.0440	0.92
	400	0.00571	-0.0831	0.72
	640	0.01119	-0.1934	0.83

Table 5.6a Dependence of DR_0 on r_L CFG.2 $DR_0 = a + br_L$

D(m)	$q \text{ (kgm}^{-3}\text{)}$	a	b	R
0.05	80	0.00346	-0.0171	0.48
	160	0.00304	-0.0071	0.12
	240	0.00302	-0.0097	0.40
	320	0.00309	0.0025	0.05
	400	0.00755	-0.1154	0.86
	640	0.01434	-0.2487	0.69
0.10	80	0.00240	-0.0259	0.76
	160	0.00210	-0.0184	0.32
	240	0.00174	-0.0010	0.03
	320	0.00184	-0.0069	0.14
	400			
	640			
0.15	80	0.00221	-0.0264	0.89
	160	0.00313	-0.0552	0.88
	240	0.00255	-0.0385	0.85
	320	0.00172	-0.0165	0.76
	400	0.00305	-0.0409	0.21
	640			

Table 5.6b Dependence of DR_0 on r_L

CF6.1 $DR_0 = a + bD$

r_L	$q \text{ (kgm}^{-3}\text{)}$	a	b	R
0	80	0.00427	-0.0163	0.74
	160	0.00298	0.0039	0.16
	240	0.00486	-0.0125	0.98
	320	0.00781	-0.0322	0.43
	480	0.01544	-0.0693	0.64
0.03	80	0.00698	-0.0023	0.27
	160	0.00096	-0.0013	0.29
	240	0.00212	-0.0085	0.56
	320	0.00307	-0.0095	0.57
	480	0.00256	-0.0051	0.65
0.06	80	0.00342	-0.0218	0.52
	160	0.00623	-0.0432	0.78
	240	0.00419	-0.0235	0.89
	320	0.00530	-0.0235	0.51
	480	0.00156	0.0022	0.17
	640	0.00479	-0.0250	0.85

Table 5.7a Dependence of DR_0 on DCF6.2 $DR_0 = a + bD$

r_L	$q \text{ (kgm}^{-3}\text{)}$	a	b	R
0	80	0.00419	-0.0133	0.82
	160	0.00305	0.0038	0.12
	240	0.00307	-0.0034	0.22
	320	0.00437	-0.0172	0.63
	480	0.01171	-0.0544	0.99
0.03	80	0.00428	-0.0316	0.50
	160	0.00166	-0.0083	0.73
	240	0.00180	-0.0095	0.76
	320	0.00274	-0.0141	0.72
	480	0.00335	-0.0169	0.64
0.06	80	0.00332	-0.0194	0.59
	160	0.00429	-0.0255	0.77
	240	0.00372	-0.0195	0.84
	320	0.00527	-0.0225	0.70
	480	0.00255	-0.0097	0.64

Table 5.7b Dependence of DR_0 on D

CFG.1		D = 0.05			D = 0.10			D = 0.15		
η	r_L	0	0.03	0.06	0	0.03	0.06	0	0.03	0.06
80	U_0	0.4014	0.3715	0.3773	0.4101	0.3739	0.3810	0.3822	0.3939	0.3822
	$D \cdot R_0$	0.775	0.185	0.255	1.550	0.520	0.840	1.065	1.365	1.065
	β_3	-1.31	-0.16	-0.33	-8.51	-3.69	-5.86	-9.40	-19.44	-21.89
160	U_0	0.4069	0.3871	0.3887	0.4333	0.3853	0.3842	0.4030	0.3924	0.3876
	$D \cdot R_0$	0.635	0.380	0.400	2.040	0.460	0.779	0.930	0.960	0.810
	β_3	-0.87	-0.55	-0.54	-9.99	-1.60	-4.38	-7.46	-12.31	-10.07
240	U_0	0.4179	0.3947	0.3963	0.4210	0.3911	0.3967	0.4035	0.3970	0.3994
	$D \cdot R_0$	0.940	0.510	0.475	1.000	0.460	1.170	0.525	0.885	0.705
	β_3	-1.29	-0.72	-0.62	-2.95	-1.52	-5.52	-1.65	-8.20	-7.94
320	U_0	0.4260	0.4013	0.4024	0.4285	0.3991	0.3818	0.4262	0.4625	0.3877
	$D \cdot R_0$	0.930	0.559	0.589	1.120	0.570	0.400	1.440	0.795	0.630
	β_3	-1.05	-0.71	-0.77	-3.31	-1.76	-1.25	-7.88	-5.70	-5.83
480	U_0	0.4681	0.4058	0.3909	0.4416	0.4029	0.3952	0.4667	0.4436	0.3871
	$D \cdot R_0$	1.705	0.650	0.515	1.030	0.530	0.480	1.920	3.645	0.480
	β_3	-1.46	-0.85	-0.67	-1.98	-1.34	-1.24	-7.25	-32.28	-3.05
640	U_0		0.4140	0.4138	0.4621	0.4071	0.3929	0.4974	0.4120	0.3950
	$D \cdot R_0$		0.720	0.740	1.210	0.640	0.460	3.030	0.990	0.555
	β_3		-0.86	-0.91	-1.71	-1.58	-1.22	-9.07	-5.87	-3.19

Table 5.8a Results from fitting of eq (5.1) to the
measured arrival times
 $D \cdot R_0$ is multiplied by 10^3 and β_3 by 10^6

CFG.2		D = 0.05			D = 0.10			D = 0.15		
q	r _L :	0	0.03	0.06	0	0.03	0.06	0	0.03	0.06
80	U ₀	0.3910	0.3865	0.3996	0.4165	0.3887	0.3837	0.3854		0.3725
	D·R ₀	0.530	0.400	0.770	1.630	1.000	0.900	0.900		0.525
	β ₃	-0.79	-0.59	-1.51	-9.21	-7.23	-6.75	-9.08		-6.15
160	U ₀	0.4043	0.3887	0.3973	0.4050	0.3933	0.3922	0.4021	0.3816	0.3759
	D·R ₀	0.685	0.360	0.540	0.780	1.110	0.700	1.080	0.945	0.285
	β ₃	-0.93	-0.51	-0.76	-2.87	-7.87	-2.62	-8.03	-13.74	-0.70
240	U ₀	0.4162	0.3788	0.4004	0.4325	0.3789	0.4077	0.4138	0.3780	
	D·R ₀	0.765	0.340	0.540	1.200	0.270	0.790	1.365	0.435	
	β ₃	-0.91	-0.53	-0.69	-3.06	-0.85	-2.61	-8.86	-2.89	
320	U ₀	0.4383	0.4004	0.4090	0.4209	0.3837	0.4026	0.4107	0.3860	0.3880
	D·R ₀	1.045	0.535	0.990	0.670	0.330	0.590	0.915	0.630	0.465
	β ₃	-1.04	-0.69	-0.89	-1.45	-0.94	-1.56	-4.55	-4.99	-3.14
480	U ₀	0.4853	0.4122	0.4205	0.4363	0.3962	0.3963	0.4381	0.3879	0.3894
	D·R ₀	1.925	0.640	0.775	0.960	0.460	0.460	1.305	0.510	0.675
	β ₃	-1.41	-0.77	-0.92	-1.79	-1.19	-1.15	-4.96	-2.87	-3.92
640	U ₀	0.5425	0.4184	0.4202	0.4650					
	D·R ₀	3.550	0.670	0.665	1.460					
	β ₃	-1.96	-0.72	-0.72	-2.26					

Table 5.8b Results from fitting of eq (5.1) to the
measured arrival times
D·R₀ is multiplied by 10³ and β₃ by 10⁶

CFG.1

$$U_0 = a \cdot e^{bq}$$

r_L	D(m)	a	b	R
0	0.05	0.3339	0.000383	0.97
	0.10	0.4114	0.000134	0.91
	0.15	0.3694	0.000456	0.98
0.03	0.05	0.3743	0.000172	0.93
	0.10	0.3772	0.000134	0.91
	0.15	0.3869	0.000184	0.68
0.06	0.05	0.3791	0.000136	0.91
	0.10	0.3823	0.000051	0.59
	0.15	0.3831	0.000041	0.80

Table 5.9a Dependence of U_0 on q

CFG.2

$$U_0 = a \cdot q^{bq}$$

r_L	D(m)	a	b	R
0	0.05	0.3667	0.000593	0.99
	0.10	0.4020	0.000204	0.89
	0.15	0.3809	0.000286	0.96
0.03	0.05	0.3768	0.000166	0.89
	0.10	0.3853	0.000029	0.25
	0.15	0.3757	0.000067	0.79
0.06	0.05	0.3930	0.000115	0.94
	0.10	0.3898	0.000076	0.50
	0.15	0.3631	0.000132	0.52

Table 5.9b Dependence of U_0 on q

CFG.1

$$v_0 = a + b r_L$$

D(m)	q (kgm ⁻³)	a	b	R
0.05	80	0.3355	-401.7	0.76
	160	0.4033	-303.3	0.83
	240	0.4138	-360.0	0.83
	320	0.4217	-393.3	0.85
0.10	480	0.4589	-1153.3	0.91
	640	0.4142	-6.67	r _L = 0 missing
	80	0.4079	-585.0	0.78
	160	0.4208	-818.3	0.91
0.15	240	0.4151	-405.0	0.76
	320	0.4265	-778.3	0.89
	480	0.4364	-773.3	0.93
	640	0.4553	-1153.3	0.95
0.15	80	0.3861	0	0
	160	0.4020	-256.7	0.96
	240	0.4040	-235.0	0.99
	320	0.4234	-808.3	0.98
0.15	480	0.4684	-1226.7	0.93
	640	0.4863	-1706.7	0.94

Table 5.10a Dependence of v_0 on r_L

CFG.2

$$u_0 = a + b r_L$$

D(m)	q (kgm ⁻³)	a	b	R
0.05	80	0.3862	143.3	0.66
	160	0.4003	-116.7	0.45
	240	0.4304	-203.3	0.42
	320	0.4306	-488.3	0.74
0.10	480	0.4717	-1080.0	0.81
	640	0.5215	-2038.3	0.86
0.15	80	0.4127	-546.7	0.93
	160	0.4032	-213.3	0.90
	240	0.4168	-413.3	0.46
	320	0.4115	-301.7	0.49
0.15	480	0.4309	-675.0	0.86
	80	0.3864	-231.7	r _L = 0.03 missing
	160	0.3996	-436.7	0.95
	240	0.4138	-1163.3	r _L = 0.06 missing
0.15	320	0.4063	-378.3	0.83
	480	0.4285	-811.7	0.85
0.15	640			

Table 5.10b Dependence of u_0 on r_L

CFG.1		$U_0 = a + bD$			CFG.2		$U_0 = a + bD$		
r_L	$q \text{ (kgm}^{-3}\text{)}$	a	b	R	r_L	$q \text{ (kgm}^{-3}\text{)}$	a	b	R
0	80	0.4191	-192.0	0.55	0	80	0.4026	-46.0	0.14
	160	0.4193	-39.0	0.12		160	0.4060	-22.0	0.73
	240	0.4265	-144.0	0.77		240	0.4232	-24.0	0.12
	320	0.4200	102.0	0.96		320	0.4509	-276.0	0.93
	480	0.4642	-74.0	0.27		480	0.5006	-472.0	0.85
0.03	80	0.3574	224.0	0.91	0.03	80	0.3951	36.0	D=0.15 missing
	160	0.3843	53.0	1.00		160	0.3950	-71.0	0.50
	240	0.3914	31.0	0.46		240	0.3794	-8.0	0.31
	320	0.3991	22.0	0.50		320	0.4044	-144.0	0.80
	480	0.3763	428.0	0.84		480	0.4231	-243.0	0.96
0.06	80	0.3753	49.0	0.95	0.06	80	0.4124	-271.0	1.00
	160	0.3879	-11.0	0.23		160	0.4099	-214.0	0.96
	240	0.4010	-69.0	0.84		240	0.3931	146.0	D=0.15 missing
	320	0.4053	-147.0	0.69		320	0.4203	-210.0	0.97
	480	0.4055	-118.0	0.98		480	0.4332	-311.0	0.95

Table 5.11a Dependence of U_0 on D Table 5.11b Dependence of U_0 on D

CFG.1

$$R_0 D = a \cdot e^{bq}$$

r_L	D(m)	a $\times 10^5$	b	R
0	0.05	0.55	0.00211	0.91
	0.10	1.61	-0.00071	0.53
	0.15	0.61	0.00233	0.80
0.03	0.05	0.24	0.00202	0.95
	0.10	0.46	0.00046	0.74
	0.15	0.99	0.00067	0.25
0.06	0.05	0.30	0.00148	0.87
	0.10	0.98	-0.00135	0.67
	0.15	1.00	-0.00115	0.88

Table 5.12a Dependence of DR on q

CFG.2

$$R_0 D = a e^{bq}$$

r_L	D(m)	a $\times 10^3$	b	R
0	0.05	0.35	0.00342	0.99
	0.10	1.03	0.00010	0.06
	0.15	0.93	0.00064	0.59
0.03	0.05	0.33	0.00120	0.97
	0.10	1.01	-0.00247	0.55
	0.15	0.89	-0.00130	0.53
0.06	0.05	0.62	0.00018	0.23
	0.10	1.01	-0.00166	0.94
	0.15	0.35	0.00116	0.57

Table 5.12b Dependence of DR on q

CFG.1 $R_0 D = a + b r_L$

D(m)	q (kgm ⁻³)	a X10 ³	b	R
0.05	80	0.67	-8.7	0.81
	160	0.61	-4.2	0.83
	240	0.87	-7.8	0.90
	320	0.86	-5.8	0.83
	480	1.55	-13.8	0.91
	640	0.70	0.7	$r_L = 0$ missing
0.10	80	1.33	-11.3	0.67
	160	1.73	-21.2	0.76
	240	0.79	2.8	0.23
	320	1.66	-12.0	0.96
	480	0.96	-9.2	0.90
	640	1.15	-12.5	0.96
0.15	80	1.17	0	0
	160	0.96	-2.0	0.76
	240	0.63	3.0	0.50
	320	1.36	-13.5	0.95
	480	2.73	-24.0	0.45
	640	2.76	-41.3	0.94

Table 5.13a Dependence of DR_0 on r_L

CFG.2 $R_0 D = a + b r_L$

D(m)	q (kgm ⁻³)	a X10 ³	b	R
0.05	80	0.45	4.0	0.64
	160	0.61	-2.4	0.48
	240	0.66	-3.8	0.53
	320	0.93	-5.9	0.68
	480	1.60	-19.2	0.81
	640	3.37	-48.1	0.87
0.10	80	1.54	-12.2	0.92
	160	0.50	-1.3	0.16
	240	0.96	-6.8	0.44
	320	0.57	-1.3	0.23
	480	0.83	-8.3	0.67
	640			
0.15	80	0.90	-6.3	$r_L = 0.03$ missing
	160	1.17	-13.2	0.93
	240	1.37	-31.0	$r_L = 0.06$ missing
	320	0.90	-7.5	0.99
	480	1.14	-10.5	0.75
	640			

Table 5.13b Dependence of DR_0 on r_L

CF6.1

 $R_0 D = a + bD$

r_L	$q \text{ (kgm}^{-3}\text{)}$	$a \times 10^3$	b	R
0	80	0.840	2.50	0.37
	160	0.947	2.65	0.18
	240	1.237	-4.15	0.80
	320	0.653	5.10	0.99
	480	1.337	2.15	0.23
0.03	80	-0.490	11.80	0.97
	160	0.020	5.80	0.92
	240	0.243	3.75	0.81
	320	0.393	2.45	0.90
	480	-1.387	29.95	0.35
0.06	80	0.513	2.70	0.74
	160	0.030	8.10	0.97
	240	0.250	4.10	0.91
	320	0.553	2.30	0.32
	480	0.487	0.50	0.21
		0.527	-0.35	0.87
		0.770	-1.85	0.65

Table 5.14a Dependence of DR_0 on D

CF6.2

 $R_0 D = a + bD$

r_L	$q \text{ (kgm}^{-3}\text{)}$	$a \times 10^3$	b	R
0	80	0.630	3.70	0.33
	160	0.453	3.95	0.96
	240	0.510	6.00	0.97
	320	1.007	-1.30	0.34
	480	2.017	-0.20	0.63
0.03	80	-0.200	12.00	$D=0.15$ missing
	160	0.247	5.65	0.74
	240	0.253	0.95	0.57
	320	0.403	0.95	0.31
	480	0.667	-1.30	0.70
0.06	80	0.977	-2.45	0.64
	160	0.793	-2.55	0.61
	240	0.290	5.00	$D=0.15$ missing
	320	0.807	-2.25	1.00
	480	0.737	-1.00	0.31

Table 5.14b Dependence of DR_0 on D

CFG.1

$$X = a q^b$$

r_L	D(m)	a	b	R
0	0.05	13.94	0.41	0.94
	0.10	12.23	0.43	0.98
	0.15	14.85	0.40	0.97
0.03	0.05	14.84	0.36	0.92
	0.10	9.95	0.45	0.80
	0.15	20.81	0.31	0.94
0.06	0.05	13.00	0.35	0.92
	0.10	12.32	0.40	0.95
	0.15	15.77	0.38	0.84

Table 6.2a Dependence of X on q

CFG.2

$$X = a q^b$$

r_L	D(m)	a	b	R
0	0.05	6.66	0.57	0.95
	0.10	6.03	0.60	0.96
	0.15	5.47	0.61	0.96
0.03	0.05	10.18	0.44	0.89
	0.10	2.72	0.73	0.75
	0.15	11.94	0.45	0.91
0.06	0.05	12.34	0.40	0.92
	0.10	2.04	0.76	0.87
	0.15	30.30	0.30	0.69

Table 6.2b Dependence of X on q

CFG.1		$X = a + b r_L$			CFG.2		$X = a + b r_L$		
D(m)	q (kgm ⁻³)	a	b	R	D(m)	q (kgm ⁻³)	a	b	R
0.05	80	81	-283	0.61	0.05	80	32	-158	0.48
	160	122	-833	0.95		160	112	-239	0.64
	240	121	-483	0.81		240	140	-673	0.64
	320	138	-772	0.75		320	191	-1522	0.82
	480	168	-833	0.92		480	217	-1233	0.82
0.10	640	196	-1245	0.95	0.10	640	241	-1350	0.63
	80	82	-203	0.43		80	84	-495	0.50
	160	105	-74	0.12		160	129	17	0.61
	240	126	-110	0.13		240	175	-403	0.62
	320	154	-446	0.56		320	187	-822	0.55
0.15	480	181	-650	0.78	0.15	480			
	640					640			
	80	85	-147	0.44		80	90	64	0.30
	160	109	496	0.60		160	193	760	0.84
	240	128	57	0.07		240	139	617	0.70
0.15	320	157	-732	0.68	0.15	320	190	-433	0.34
	480	156	-55	0.19		480	251	-1522	0.95
	640	182	-161	0.25		640			

Table 6.3a Dependence of X on r_L Table 6.3b Dependence of X on r_L

CFG.1

CFG.2

X = a + bD				
r _L	q (kgm ⁻³)	a	b	R
0	80	81	18	0.15
	160	123	-139	0.52
	240	110	193	0.72
	320	129	233	0.57
	480	139	-153	0.39
0.03	640	204	-107	0.47
	80	60	133	0.35
	160	102	10	0.03
	240	107	57	0.14
	320	106	153	0.31
0.06	480	128	147	0.54
	640	152	20	0.13
	80	61	97	0.40
	160	67	362	0.53
	240	63	487	0.83
	320	84	309	0.62
	480	111	324	0.92
	640	95	580	0.92

Table 6.1a Dependence of X on D

X = a + bD				
r _L	q (kgm ⁻³)	a	b	R
0	80	80	67	0.50
	160	115	-47	0.22
	240	159	-40	0.09
	320	205	-45	0.10
	480	220	220	0.90
0.02	640			
	80	83	-170	0.21
	160	118	66	0.06
	240	83	531	0.55
	320	110	303	0.77
0.06	480	123	470	0.81
	640			
	80	52	195	0.35
	160	65	547	0.91
	240	72	737	0.87
	320	96	513	0.63
	480	149	90	0.52
	640			

Table 6.1r Dependence of X on D

	D(m)	SCALE	Q	$q = \frac{Q}{D^3}$	No of measurement positions included in curve fitting	$P = P_0 \left(\frac{N}{20}\right)^{-B}$		
						P_0	B	R
STORFOSEN	4.00	80:100	72.4	1.13	4	0.034	1.355	0.94
STORFOSEN	4.00	80:100	375.3	5.86	5	0.097	1.434	0.98
STORFOSEN	2.85	57:100	151.3	6.40	2	0.033	1.293	—
STORFOSEN	2.85	57:100	302.5	12.07	2	0.053	1.128	—
STORFOSEN	2.85	57:100	1495	64.1	2	0.140	0.993	—
RAUFOSS	2.65	53:100	100	5.37	4	0.033	0.984	1.00
RAUFOSS	2.65	53:100	300	16.12	2	0.046	1.073	—
RAUFOSS *	2.65	53:100	1000	53.7	3	0.096	1.315	0.95
RAUFOSS *	2.65	53:100	1000	53.7	3	0.065	1.130	0.98

* The charges are placed at different distances from the closed end of the tunnel.

Table 7.1 Results from some Norwegian full scale tests